The effect of concurrent radiation and calcium in two cancer cell lines

Jessica Billberg

Supervision

Faisal Mahmood and Stine Krog Frandsen

This work has been performed at
Department of Oncology, Herlev and Gantofte Hospital, University
of Copenhagen, Denmark

Department of Medical Radiation Physics,
Clinical Sciences, Lund
Lund University

Abstract

Introduction Calcium is an important ubiquitous second messenger regarding the maintenance of cellular homeostasis, and is therefore tightly regulated. Calcium induces cell death when internalised into cancer cells after permeabilization of the cell membrane by electroporation. It is established that radiation causes damage to the lipids and proteins of the cell membrane; and ionizing radiation also causes permeabilization of the cell membrane by peroxidation of the phosphor-lipid layer.

Purpose To investigate the survival of two cancer cell lines exposed to high levels of calcium in combination with radiation.

Materials and Methods Two human cancer cell lines were used in this study; H69 (small cell lung cancer) and SW780 (bladder cancer). Using an x-ray system (Gulmay D3100, Gulmay medical) 30.000 cells in 50 µl hepes buffer with or without 5mM $CaCl_2$ was irradiated in open air with x-rays of 100 kVp and half value layer (HVL) of 5.2 mm aluminum in the dose range of 0-16 Gy. The survival rate was first and foremost assessed using a MTS viability assay, however clonogenic assay was also used to assess the survival after irradiation performed with a Varian 2300iX Clinic linear accelerator (Varian Medical Systems,Inc., Palo Alto, CA). To verify the given dose, GAFCHROMIC^{TM} EBT3 dosimetry film and TLD were used.

Result No difference in cell viability of SW780 and H69 cells treated with or without calcium in combination with radiation could be detected when using MTS viability assay to determine the cell survival rate. No dose response was obtained. When using clonogenic assay, the result displayed no difference in viability of the cells treated with or without calcium, however a cellular response to an increased absorbed dose could be distinguished. Results from measurements performed with EBT3 dosimetry film and TLDs assured the dose delivery to the cells in this study.

Conclusion. The effect of concurrent radiation and calcium could not be investigated properly due to the method chosen for determination of cell survival. It is therefore necessary to continue to investigate the effect of calcium in combination with radiotherapy, tentatively using clonogenic assay to determine cell viability after treatment, before further conclusions are drawn.

Popular scientific summary in Swedish

Elektroporation är, på Herlevs sjukhus i Danmark, en relativt vanlig metod för att behandla olika typer av hudcancer eller andra cancerformer som utgår från en ytligt belägen mjukvävnad. Behandlingsmetoden använder sig av korta högspänningspulser som överstiger cellmembranets potential, vilket resulterar i att cellmembranets permeabilitet förändras under en kort tid. Är joner eller andra molekyler närvarande under behandlingen kan inflödet av dessa öka och därigenom påverka cellerna. Vidare forskning, både *in vitro* och *in vivo*, har påvisat att elektroporation vid närvaro av kalcium (s.k. kalcium elektroporation) minskar cellöverlevnaden drastiskt då cellerna dör till följd av energiutarmning. Denna studie undersöker således om den permeabilisering av cellmembranet som sker när cellerna utsätts för joniserande strålning är tillräcklig för att öka inflödet av kalcium och därmed påverka cellöverlevnaden hos småcellig lungcancer- och blåscancerceller. Syftet med studien är följaktligen att undersöka den samverkande effekten av kalcium och strålbehandling hos två cancercellslinjer samt verifiera den absorberade dosen till cellerna.

I denna studie användes två olika cancercellinjer, SW780 (blåscancer) och H69 (småcellig lungcancer). Suspension innehållandes 30 000 celler utspädda i hepes-buffer med eller utan 5mM $CaCl_2$, bestrålades med röntgenstrålar med en rörspänning på 100 kVp och en halvvärdestjocklek på 5,2 mm aluminium genererade av en röntgenapparat (Gulmay D3100,Gulmay Medical) på Herlev sjukhus. De absorberade doser som cellerna erhöll var mellan 0 och 16 Gy och två dagar efter bestrålningen analyserades cellöverlevnadsgraden med hjälp av MTS. För att utvärdera MTS analysen utfördes ett experiment där cellöverlevnadsgraden bestämdes med hjälp av en klonogen analys (clonogenic assay). Den absorberade dosen som cellerna erhöll verifierades med hjälp av mätningar med GAFCHROMIC™ EBT3 film och TLD.

Det resultat som erhölls för båda cellinjer påvisade ingen skillnad i överlevnadsgrad för celler som behandlats med och utan kalcium i kombination med strålbehandling. Ingen reducerad cellöverlevnad till följd av en ökande absorberad dos kunde konstateras då cellöverlevnaden analyserades med MTS. En dosrespons kunde dock påvisas då cellöverlevnaden analyserades med hjälp av en kolonogen analys. Mätningarna som utfördes med GAFCHROMIC™ EBT3 film och TLD verifierade och säkerställde den absorberade dosen till cellerna i de olika bestrålningsgeometrierna.

För de två cellinjerna som användes i den här studien kunde ingen skillnad i överlevnadsgrad mellan kalcium- och icke-kalciumbehandlade celler som bestrålats påvisas då cellöverlevnaden undersöktes genom en analys med MTS. På grund av den metod som valts för att avläsa cellöverlevnadsgraden kunde inte den samverkande effekten av strålbehandling och kalcium utvärderas fullständigt. Det är möjligt att en samverkande effekt mellan strålbehandling och kalcium existerar, men den har inte kunnat observeras med den valda analysmetoden i den här studien. Därför är det nödvändigt att vidare utvärdera den samverkande effekten av strålterapi och kalcium, förslagsvis med en klonogen analys, innan en slutgiltig slutsats dras.

Abbreviations and acronyms

ANOVA…………………………………………………………….……Analysis of Variance

ATP……………………………………………………......……………..Adenosine Triphosphate

dpi…………………………………………………………………………...Dots per inch

DNA…………………………………………………………...….…..Deoxyribonucleic Acid

FSD………………………………………………………..…………Focus to Skin Distance

Gy………………………………………………..…………………Gray, unit of absorbed dose

H69 cells……………………………………………………………Small cell lung cancer cells

HVL…………………………………………………………………...Half Value Layer

LET……………………………………………………………………Linear Energy Transfer

LC……………………………………………………………………Luminescence Centres

MTS………………….....…3-(4,5-dimethylthiazol-2-yl)-5-(carboxymethophenyl)-2-(4-sulfonyl)-2H-tetrazolium

OD……………………………………..…………………………………Optical Density

PBS………………………………………………………………….Phosphate-Buffered Saline

PE………………………………………………………………….....Plating Efficiency

PMMA…………………………………………...……………………Polymethylmethacrylate

PTP……………………………………………………………………Permeability Transition Pores

PUFA………………………………………………………………….Polyunsaturated Fatty Acid

ROI…………………………………………………………………Reactive Oxygen Intermediates

ROS…………………………………………………………………Reactive Oxygen Species

RSD…………………………………………………………….Relative Standard Deviation

SF…………………………………………………………………..Survival Fraction

SSD……………………………………………………………..Source Surface Distance

SW780 cells……………………………………………………….Bladder cancer cells

TC…………………………………………………………………Trapping Centres

TLD………………………………………………………………Thermoluminescent Dosimeter

Table of content

1. Introduction

All living things consist of cells that interact, connect, and form tissues, organs, and organ systems. The cell is a world in itself and the human cell is, together with the generated products of the cell and fluids, the fundamental element of a human being [1]. An adult human body consist of approximately 75 trillion cells and though all human cells have much in common there are many characteristics such as different size, shape, and function that set them apart [1]. This creates a problem in describing the characteristic human cell and therefore is a composite cell that includes known cell structures presented in Figure 1.
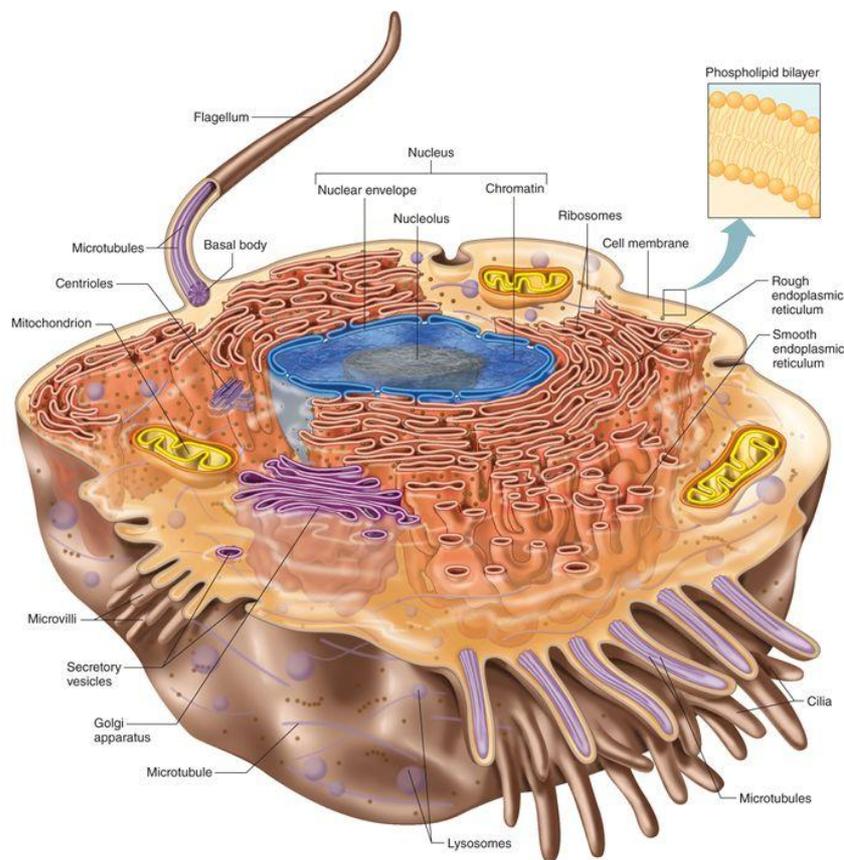

Figure 1. The general charactheristics and structures of a composite human cell [1].

The human cell can be divided into three main parts; nucleus, cytoplasm and cell membrane [1]. A characteristic human cell that is not going through mitosis has one nucleus that controls the cellular activity and houses the genetic material. Cytoplasm is a gel-like material that fills out the cell and is the medium organelles and specialized structures are suspended in. The cell membrane encloses the cell and defines it.

When a substance is irradiated by photons the energy deposition depends of the energy of the photons and the chemical composition of the target. For x-ray photons of about 100 kVp interactions by the photoelectric effect is dominating [2], [3]. Damage to biological materials when irradiated occurs essentially as damage to the deoxyribonucleic acid (DNA), also known as the critical target. There are two ways that radiation can cause damage to the DNA, direct action and indirect action. Direct action

occurs when the radiation interacts directly with the critical target and ionizes or excites its atoms. This starts the chain of events that leads to biological change by creating DNA radicals which results in breaking of chemical bounds in DNA [3]. Direct action is dominating when the radiation consists of high linear energy transfer particles (LET), such as α-particles and neutrons. Indirect action occurs when the radiation interacts with other molecules or atoms in the cell, regularly water, thus producing free radicals within the cell [3]. These radicals can diffuse a short distance, reach the critical target and thereby generate DNA radicals, resulting in disruptions of the chemical bonds in DNA. Approximately 70 % of all biological damage that occur through interactions between x-rays and biological materials are due to indirect action [3]. Apart from causing damage to the DNA, which may initiate cell death in itself, radiation can trigger several other mechanisms including; mitotic and apoptotic death, the bystander effect, autophagic cell death, senescence, and oxidative stress response (ROS) derived from the intercellular water [3]–[6].

Calcium is an important substance that acts as a second messenger in the cell and is involved in numerous cellular processes, such as proliferation, muscle contraction, transcription, and metabolism [7]–[10]. Due to the big impact of calcium regarding the maintenance of cellular homeostasis, the calcium concentration is extremely regulated. The extracellular calcium concentration is approximately 1 mmol/L and the intracellular calcium concentration is approximately 0.1 µmol/L [10]. Mechanisms that regulate the calcium concentration are therefore extremely important for maintaining the cellular homeostasis. Ca^{2+}-ATPase is the membrane pump that contribute to maintaining a low intracellular calcium concentration, and thereby regulates the cellular homeostasis by consuming adenosine triphosphate (ATP) [11]. An increased intracellular calcium concentration will result in an increased activity of Ca^{2+}-ATPases and affect the mitochondria by eliminating the mitochondrial formation of new ATP, thus resulting in ATP depletion and cell death [10], [12], [13]. By combining electroporation, where the cell membrane is permeabilized by exposing the cells to short high-voltage pulses, and calcium injections the intracellular concentration of free calcium is increased and the cell viability is decreased [10], [11], [14]. An increase in the intracellular concentration of free calcium may induce cell death through necrosis and apoptosis [15] and after treatment with calcium electroporation cells die through necrosis [10].

It is established that radiation affects the cell membrane; it causes damage to lipids and membrane proteins resulting in cell necrosis and metabolic exhaustion [16], [17]. An increase of ion permeability of the plasma membrane after ionizing radiation has also been observed [12], [18], [19]. The hypothesis is that by exposing cancer cells to calcium and ionizing radiation the intracellular concentration of calcium may increase as a result of the increased ion permeability, resulting in increased cell mortality due to energy depletion. Thus, substituting calcium for chemotherapeutic agents could be efficient and inexpensive. The purpose of this project is consequently to

- Study the concurrent effect of calcium and radiotherapy in two cancer cell lines by comparing the survival fraction between cells that are treated with and without calcium and irradiated,
- Study if the potential effect of calcium on the survival of the cells is influenced by the absorbed dose,
- Verify the delivered doses to the cells using EBT3 Dosimetry film and TLDs.

2. Theory

2.1   Cell death and cellular response to radiation

2.1.1   Mechanisms of cell death

Cell death is usually defined as the permanently loss of the ability to proliferate indefinitely or, for differentiated types of cells, loss of function [3], [6]. Cell death occurs by several different mechanisms, however the pathways that initiate the different programmed forms of cell death are frequently altered in cancer cell lines, thus cancer cells are able to endure a higher level of stress than normal cells [6].

Apoptosis is a programmed form of cell death that is strictly controlled and can be initiated by internal or external conditions. It may be initiated as a part of the DNA damage response system and even though the DNA repair mechanisms are activated the cell will die following the activation of apoptosis pathways [6]. This cell death mechanism is only active within fast proliferating cells, e.g. lymphocytes, thymocytes, or cancer cells that arise from these cell lines [3], [6]. As a result this kind of cell death is seldom seen in solid tumours [6]. When apoptosis is initiated several morphological characteristics are notable; membrane blebbing, condensation of chromatin, digestion of DNA and phagocytes that digest fragmented membrane-enclosed cellular contents (known as apoptotic bodies) [3], [6]. Genes, e.g. p53, that initiate apoptosis may be altered in cancer cells, therefore these cells are unable to initiate apoptosis and have thus a reduced apoptotic sensitivity [6].

Another mechanism of cell death is autophagy, i.e. a process where the cell digests parts of the cytoplasm in order to maintain the cellular homoeostasis by generating small macromolecules and energy [3], [6]. The autophagy mechanism is controlled by gene products that initiate the formation of membrane structures that engulf cytoplasmic components, thus vacuoles containing cytoplasm, known as autophagasomes, are created. Lysosomes and autophagasomes fuse together and generation of the enclosed material into energy and primary components is initiated [6]. Activation of autophagy may lead to cell death, however some cancer cells have lost the function of the genes that initiates the process, resulting in a higher endurance to unfavourable conditions [6].

Necrosis have for long been considered an uncontrolled, random and chaotic form of cell death that is irreversible [3], [6]. Evidence supporting the idea of key mediators in the necrotic death have however established the term "programmed necrosis" or type III programmed cell death [20]. It can be initiated by exposure to ionizing radiation and general characteristics for a cell that is undergoing necrosis are cellular swelling, membrane deformation, organelle breakdown, and release of lysosomal enzymes [3], [6].

In normal cells the telomeres are gradually shortening when the cell is undergoing mitosis, eventually resulting in a permanent loss of ability to divide. These cells that have lost their ability to divide do not necessarily display a loss of function and may remain metabolic intact, this mechanism of cell death is known as senescence [3], [6]. This state of permanently cell cycle arrest may be initiated by exposing cells to stress conditions, e.g. exposing them to radiation and thereby inducing damage to the DNA. Genetic changes in cancer cells may affect the pathways that control senescence, thereby manipulating the cell to continue to divide [6].

The main reason for cell death after irradiation is considered to be mitotic cell death [3], [6]. Due to unrepaired DNA or errors in the reparation the cell fails to correctly complete mitosis. Cell death follows as a result of the inability to separate and replicate the DNA or due to the loss of genetic material associated with the mitotic process [3], [6]. After exposure to radiation the DNA repair system and cell cycle checkpoints are activated as a response. Mitotic cell death occurs after cell cycle checkpoints are inactivated and when the reparation of the DNA is completed to a large extent [6]. Cell death follows as a result of the cell not being able to properly complete mitosis and not due to the damages generated by radiation. Morphological characteristics are giant cells containing uncondensed chromosomes and the presence of chromosomes aberrations [6]. Several authors have investigated the quantitative relationship between specific chromosomal aberrations and cell death, e.g. Cornforth et al. [21] found that there are one-to-one correlation between asymmetric exchange-type aberrations and cell death. Even though the results in these studies are circumstantial, they provide evidence that radiation induced mitotic cell death may be initiated by chromosomal asymmetric exchange-type aberrations. Genes that are involved in the mitotic checkpoints activation may be altered in cancer cells, thereby altering their ability to undergo mitotic cell death [6]. Usually it takes two or more cell cycles for the cells to die by mitotic cell death, however it may cause enough damage to trigger other cell death mechanisms such as senescence, apoptosis and autophagy [3], [6].

The cell death mechanisms can be divided into two categories; early cell death that occurs before cell division and late cell death that occur relatively late during mitosis or after [6]. Pre-mitotic cell death occurs within hours after exposing cells to stress conditions, e.g. exposure to ionizing radiation. The cause of pre-mitotic cell death is primarily the activation of pathways in response to the radiation-induced damages to the DNA. Apoptosis, autophagy, necrosis, and senescence are all examples of cell death mechanisms that are responsible for cells dying at an early stage after irradiation. A majority of proliferating normal and cancer cells die relatively long time after irradiation; regularly post-mitotic cell death occurs after one or more cell cycles [6]. Mitotic cell death is regarded as the only post-mitotic cell death mechanism, however it may initiate pre-mitotic cell death mechanisms e.g. apoptosis and senescence.

2.1.2 Generation of ROS/ROI and oxidative stress

Reactive Oxygen Species (ROS) or Reactive Oxygen Intermediates (ROI) are chemically reactive molecules that are enriched with one or more oxygen atoms, e.g. O_2^-, HO_2^-, $OH^\cdot$ and H_2O_2 [4]. Cells produce ROS at a moderate concentration during normal physiological conditions and they participate in signalling pathways that regulate expression of specific genes and modulate ion channel activities [22]. A moderate concentration of ROS can thus stimulate cell proliferation and differentiation while an abnormal level of ROS will function as a toxic agent, causing oxidative damage [4], [22]. At high concentrations, ROS are considered to be the main cause for oxidizing events that alter the atomic structure of macromolecules, which is known as oxidative stress [4], [22]. The concentration of ROS are therefore tightly regulated in order to maintain the homeostatic cellular functions [4], [22].

ROS/ROI and thereby oxidative stress can also be generated by ionizing radiation [22]. ROS are generated in the cells and the extracellular space within days and months after the initial exposure [23], moreover the irradiated cells' progeny will also generate ROS [22]. For low LET radiation, e.g. x-rays, the indirect effect, leading to radiolysis of the cellular water and generation of ROS, is the most common way for the radiation to interact with biologic material [3], [22]. Absorption of the photon or passage of the charged particle in the biologic material can be divided into four stages. In the first stage the energy deposition occur due to the incident radiation and secondary electrons are generated [4].

During the second state the highly unstable generated species reorganize, the processes produce radical and molecular products of radiolysis which are distributed in an inhomogeneous track structure. The secondary electrons slow down and becomes trapped or hydrated at thermal equilibrium [4]. In the third state the reactive species diffuse and react with their surroundings or with each other [22]. This results in formation of biological radicals (R·) through H-abstraction and the reaction is often initiated by OH· [3], [22]. Biological radicals react rapidly with O_2 and forms peroxyl radicals (RO_2) which then can abstract H· from other molecules, thereby forming hydroperoxides (ROOH), a reaction identified to be part of lipid peroxidation [22]. In the fourth and final state the cells respond to the damage induced by the generated ROS. The DNA damages that may occur are alterations, DNA breaks, base damage, destruction of sugar, and telomere dysfunction. These damages, if unrepaired or not repaired properly will end in mutations, cell death or abnormal tissue growth [22]. Oxidative stress induced by radiation may spread by intercellular communications mechanisms from primary exposed cells to non-target bystander cells. The progeny of these cells will experience oxidative damages, e.g. enhanced rates of spontaneous gene mutations and/or protein carbonylation. This long-term effect of exposure to ionizing radiation is a long-term health risk, considering a secondary malignancy caused by radiotherapy treatment [22].

The response of normal cells to an increased concentration of ROS is initiating antioxidation reactions that decrease the cellular concentration of ROS, including release of antioxidant enzymes and down regulation of oxidative metabolism in order to lower the concentration of chemical reactive species [4], [22]. Regardless of these defence mechanisms that are triggered at high concentrations of ROS the cell will not survive an excessive increase, however many types of cancer cells have an increased tolerance towards high levels of ROS. ROS-scavenging enzymes levels are altered in malignant cells and they can therefore endure stress conditions better than normal cells [4].

2.2   Cell membrane

2.2.1   General characteristics

The cell membrane is an active part of the human cell and its main task is to control the movement of substances that enter and leave the cytosol. It consists of a double layer of phospholipid molecules, that are infiltrated with cholesterol, proteins and carbohydrates [1]. A phospholipid molecule is a composite phosphate group and two fatty acids bound to a glycerol molecule. The water-soluble phosphate heads constitute the surface of the membrane and the fatty acids form the interior, see Figure 2. This double layer of phospholipids, also known as bilayer, is thin, flexible, and to some extent elastic [1]. Molecules that are soluble in lipids, e.g. oxygen, are able to pass the bilayer through diffusion, however water-soluble substances, e.g. proteins, ions, sugars and nuclei acids, can only pass the membrane through active or passive transport channels [1]. The ability of the cell to partly regulate the substances that enter the cytosol is described as the cell being selectively permeable.
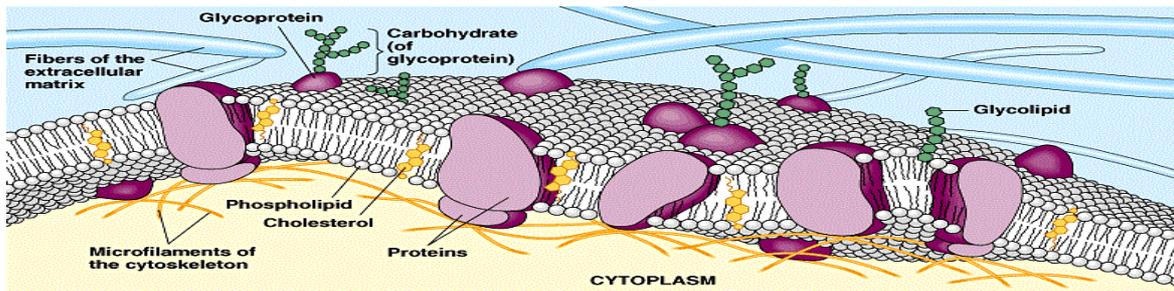
Human cell membranes are infiltrated with cholesterol which gives stability to the membranes structure and decreases permeability of water-soluble substances across the membrane. The proteins that are infiltrated in the membrane have different functions and may be classified by their positions, e.g. transmembrane proteins, which extend through the lipid bilayer, and peripheral membrane proteins, which are regularly associated with one side of the cell membrane [1]. Proteins of the cell membrane have several functions, they bind incoming growth factors, identify the cell by marking the cell as a part of a particular tissue or organ, or transport ions or molecules across the bilayer [1].

2.2.2   Effects of radiation on cell membrane

The lipids of the membrane are vulnerable to ROS and oxidative stress, and an increased level of ROS can alter the membrane bilayer, thereby initiating lipid peroxidation [4], [16], [18]. It is in principal the free radical OH$^\cdot$, generated by water radiolysis, that initiate and sustain lipid peroxidation of the membrane [4], [16], [19]. Radiation-induced ROS causes lipid peroxidation of polyunsaturated fatty acid (PUFA) in the plasma membranes, leading to formation of lipoperoxyl radicals (LOO$^\cdot$). The cells or tissues sensitivity to radiation depends on the grade of unsaturated fatty acids in the plasma membrane [19]. LOO$^\cdot$ radicals are highly chemically reactive and may react with other lipids or H-donors, producing lipid hydroperoxides (LOOH) [4], [16], [19]. The generated LOOHs are unstable and generates peroxyl and alkoxy radicals as they decompose [4], [16]. These radicals that are produced during lipid peroxidation have a local effect on the lipids, resulting in breakage of lipids and they may also contribute to cell cycle arrest and initiation of apoptosis [4]. Radiation-induced oxidative damage causing lipid peroxidation, breakage of lipids, and formation of reactive compounds alter the plasma membranes properties such as surface charge, lipid layer fluidity, membrane-bound enzymes, function of various receptors, and the permeability [4], [16], [18], [19]. E.g. Hannig et al. [18] have used microscopic fluorescence techniques to quantify the radiation-induced changes in cell permeability. Changes in permeability and fluidity of the plasma membrane can drastically alter the integrity of the cell, e.g. accumulation of polar products increasing the dielectric constant of the membrane interior, thus affecting the transportation of ions and charged particles across the membrane [16], [19]. It is established that an alteration to the plasma membrane permeability increase the influx of ions mainly due to crosslinking of lipid molecules [16], [17], [19].

2.3   Calcium electroporation

Electroporation is a local method of treating tumours where applications of short high-voltage pulses that exceed the dielectric strength of the cellular membrane results in reversible permeabilization of the membrane, permitting ions and molecules that are otherwise excluded to enter the cell [25]. Using electroporation in combination with injections of calcium, also known as calcium electroporation, local treatment of tumours can be performed [10]. As a result of the reversible permeabilization of the

cellular membrane in combination with an increased extracellular concentration of calcium, the intracellular concentration of calcium will increase dramatically [10]. Calcium is a ubiquitous second messenger that is constantly present in the intracellular environment as it is involved in many cellular processes, such as transcription, metabolism, muscle contraction, cell death, and proliferation [7]–[9], [26]. Due to its involvement in several processes the intracellular concentration of calcium is extremely monitored. The effect of a cellular influx of calcium depends on time, frequency, place, amplitude, and duration of the calcium signal [26]. Due to the large differences in calcium concentration in the plasma (high) and in the cell (low) the influx of calcium in the cell is tightly regulated and a small influx will alter the intracellular concentration dramatically, which may result in cell death through necrosis or apoptosis [15]. Frandsen et al. [10] used a colorimetric assay to measure the viability of the cells 1 and 2 days after calcium electroporation, and they found a decreased viability and a severely reduced ATP level for the treated cell lines, however calcium alone did not affect the viability of the cell lines tested, including the two cell lines used in this study; SW780 human bladder cancer and H69 human small cell lung cancer cell lines [11]. They suggest that the mechanistic explanation for the decreased survival is acute energy depletion due to decreased production of ATP caused by effects on the mitochondria, an increased intracellular consumption of ATP, and loss of ATP through the permeabilized membrane. A high intracellular level of calcium may lead to an opening of permeability transition pores (PTP) in the mitochondrial membrane, thereby losing the electrochemical gradient which is the driving force behind the ATP production [10]. The increased influx of free calcium and other ions, e.g. Na^+, may also increase the activity of the membrane pumps Ca^{2+}-ATPases and Na^+/K^+-ATPases respectively, thus increasing the consumption of ATP. A high calcium concentration may also affect other processes such as activation of lipases and proteases and the generation of ROS, thus affecting the cell viability [10]. Permeability of the lysosomal membrane is influenced by oxidative stress, alterations to calcium levels and p53 activation, an influx of free calcium and the thereby production of ROS may result in an intracellular acidification and release of enzymes that promote necrosis [6].

2.4   MTS viability assay

A fast and simple method to measure viability or more specific the general metabolism and the enzymatic activity of cells is to use 3-(4,5-dimethylthiazol-2-yl)-5-(carboxymethophenyl)-2-(4-sulfonyl)-2H-tetrazolium, also known as MTS [27]. A cell that is metabolic active might have lost its ability to proliferate, nonetheless it is determined as viable by this colorimetric assay. MTS consist of the yellow coloured tetrazolium compound, that is negatively charged and does not readily penetrate cells, and intermediate electron acceptor reagents that can penetrate the membrane of viable cells [27]. These reagents enter the viable cells, are reduced in the cytosol or at the surface of the cell and exit the cell reducing the tetrazolium compound, converting it into a purple coloured formazan product that can be detected with a plate reader [27]. Thus, metabolising cells will convert the yellow coloured MTS to the purple coloured formazan when cells are incubated with MTS. The absorbance of the samples is detected by a plate reader and is proportional to the number of viable cells in the sample.

2.5   Clonogenic assay

The common definition of cell death for proliferating cells is the loss of ability to divide, however if a cell after radiation treatment maintain the capability to grow into a large colony (at least 50 cells) that can be seen by the naked eye it has maintained its reproductive integrity and is thus viable [3], [28]. Cell death by mitotic death is the dominant effect after treatment with ionizing radiation, i.e. cell death does not occur until a couple of progressions through the cell cycle [3], [6]. Clonogenic assay has thus

been the golden standard in order to determine the cell survival after radiotherapy. Before or after the treatment cells are seeded out into flasks or plates at appropriate dilutions to form colonies for 1-3 weeks. After 1-3 weeks the number of colonies is determined and the plating efficiency (*PE*) for the untreated cells is calculated and used to determine the survival fraction (*SF*) of the treated cells [28].

2.6   TLD

A thermoluminescent dosimeter (TLD) consist of a material that contains a high concentration of trapping and luminescence centres (TC and LC respectively), e.g. LiF doped with Mg^{2+}- and Ti^{4+}-ions [29]. When a TLD is exposed to ionizing radiation electron hole pairs are created, since no external electrical field is applied the electrons migrate randomly in the conduction band. There the electrons are captured by TC, which have an energy level in the band gap, resulting in an accumulation of charges. The number of accumulated charges corresponds to the energy of the incident radiation. In the beginning of the exposure the build-up is linear to the absorbed dose, however a long exposure results in a decrease of free TC leading to a non-linear response [29]. The TC should preferably be deep so no signal is lost after exposure due to release of photons. The corresponding thermal migration and recombination applies for the radiation-induced holes [29].

During the read-out period the charges trapped in the TC are released by thermal or optical stimulation. Thermal stimulation involves the TLD to be heated up, this excites the trapped electrons to the condition band [29]. As the thermally liberated electrons migrate in the conduction band they are captured by various trapping centres. However it is only when a capture of an electron occurs at an LC that the electron and a trapped hole recombine, creating a thermoluminescence photon. The number of generated thermoluminescence photons reflects the deposited energy integrated over time [29].

Most TLD are plastic encapsulated, therefore occurs the read-out, i.e. the measurement of the total number of detected photons, at a temperature of 300°C in order to avoid the plastic from melting. The readout and/or a postreadout annealing depletes all TC and LC, thereby preparing the dosimeters for reuse [29]. One of the most commonly used TLD dosimeters TLD-100 or LiF, doped with ~180 ppm Mg^{2+} ions and ~10 ppm Ti^{4+} ions, is sensitive to thermal treatment both pre- and post-irradiation. Another downside is the low sensitivity and supralinearity for absorbed doses above 1 Gy, however the extent of supralinearity decreases with the energy of the photons [29].

2.7   GAFCHROMIC™ EBT3 Dosimetry Film

GAFCHROMIC™ dosimetry film have several properties, e.g. a high spatial resolution (at least 25 µm), no need for post-exposure treatment, a low energy dependence and being near tissue equivalent, that makes it a suitable method for measure and verify the given absorbed dose in external radiotherapy [30]. The active layer in EBT3 dosimetry film, that is 27 µm thick, contains the active components, marker dye and stabilizers [30]. Due to the yellow dye that is incorporated in the dosimetry film the sensitivity of the film to UV-light has decreased, however the recommendation from the manufacturer is to minimize the exposure to light. This active layer is enclosed by 120 µm transparent polyester substrate on either side, this structure eliminates the need to keep track of which side of the film that is facing the scanner during readout and also contribute to minimize the formation of Newton's rings interference patterns in the images that is acquired with a flatbed scanner [30]. Due to the shape of the particles of the components in the active layer the readout response is dependent of the scanning orientation. Using the red channel during readout one can measure absorbed doses up to 10 Gy.

3. Dose delivery and dosimetric challenges

3.1   Aims and Hypotheses

In order to study the concurrent effect of radiation and calcium it is of the greatest importance to assure the dose delivery to the cells in the different irradiation geometries. The hypothesis is that by finding optimal irradiation geometries, the absorbed dose to the cells in the primary radiation field can be assured at the same time as the dose contribution to adjacent cells can be neglected. The aim of this study is to

- Verify the delivered doses to the cells in the irradiation geometries using EBT3 dosimetry film and TLDs.

3.2   Materials and Methods

3.2.1   Sources of radiation

The irradiation experiments were conducted with Gulmay D3100 x-ray system (Gulmay Medical) and Varian 2300iX Clinic linear accelerator (Varian Medical Systems, Inc., Palo Alto, CA). With regard to x-rays, the energy, half value layer (HVL) and dose rate was 100 kVp, 5.2 mm aluminium and 2.76 Gy/min respectively. The energy, field size and dose rate used regarding the linear accelerator was 6 MV, 15.0×15.0 cm^2 and 600 MU/min respectively. Irradiations were held at Department of Oncology, Herlev hospital, Denmark.

3.2.2   GAFCHROMIC™ EBT3 Dosimetry film

3.2.2.1   Calibration

A film sample, cut to the size of 7.0×7.0 cm^2, was placed on top of 3.0 cm polymethylmethacrylate (PMMA). To obtain the calibration curve the film samples were exposed to doses between 0.0 and 8.0 Gy at an interval of 0.2 Gy. The focus to skin distance (FSD) and diameter of the circular applicator was 15 cm and 6 cm respectively and the film was irradiated perpendicular to the incident 100 kVp beam generated by an x-ray system (Gulmay D3100, Gulmay Medical). A flatbed scanner (EPSON PERFECTION 4990 PHOTO) and its associated software, PTW-FilmScan v. 2.6, was used to read the film samples and the samples were scanned in landscape orientation as was recommended by the manufacture due to lateral response artifacts. RGB-positive images were acquired using the red channel with 48 bits per channel, a spatial resolution of 75 dots per inch (dpi) and were saved in tiff-format. The raw images of the irradiated films were imported from the scanning system into PTW-FilmCal v.2.3 where the analysis and generation of the calibration curve was performed in a circular region of interest positioned in the middle of the radiation field with a diameter of 3.0 cm.

From each sample of film exposed to radiation 25 arbitrary points were chosen. Each collected point of data corresponded to the mean optical density (OD) of a 7×7 matrix within the defined region of interest of the dosimetry film. All 25 measurement points were recorded and for each sample of film the mean OD together with the relative standard deviation (RSD) i.e. the standard deviation of the sample divided with the absorbed dose, were calculated.

Borca et al. [30] have closely investigated the accuracy of EBT3 film measurements and they found that the background within a batch was less than 1%. Following their recommendation for a study, such as this one that only applied films from one batch, it was not considered necessary to determine

individual background values. The study performed by Borca et al. [30] applies the method proposed by Van Battum et al. [31] were they concluded that the scan mode, inter batch variations and intrinsic film inhomogeneity are the most prominent uncertainties in EBT film dosimetry. However, having a consistency in scan mode and applying films from the same batch avoids the two former. Both of these methods to reduce the uncertainties were applied during this study and the intrinsic film inhomogeneity was therefore considered the most prominent uncertainty. Van Battum et al. [31] have investigated the intrinsic film inhomogeneity further and recommend that the uncertainty in dose detection due to inhomogeneity is set to 1.5-5% for EBT dosimetry film.

3.2.2.2   *Assessment of different irradiation geometries*

To find the optimal irradiation geometry, i.e. to assure the delivered absorbed dose to the wells of a 96-well plate in the primary radiation field (e.g. well B2-C4) and minimizing the absorbed dose, due to scatter, to the adjacent wells (e.g. well F9-G11), different irradiation geometries were examined. The absorbed dose to the wells was evaluated using EBT3 dosimetry film. Film samples, cut to the size of 10.2×14.0 cm^2, were placed on 3.0 cm PMMA and a 96-well plate containing 50 µl hepes buffer in wells B2-C4 and F9-G11 were placed on top perpendicular to the incident 100 kVp beam generated by an x-ray system (Gulmay D3100, Gulmay Medical). A customized lead-infused rubber, with a 3.0×3.0 cm^2 hole, was placed on top of the plate exposing the wells selected to be in the primary radiation field, see Figure 3.
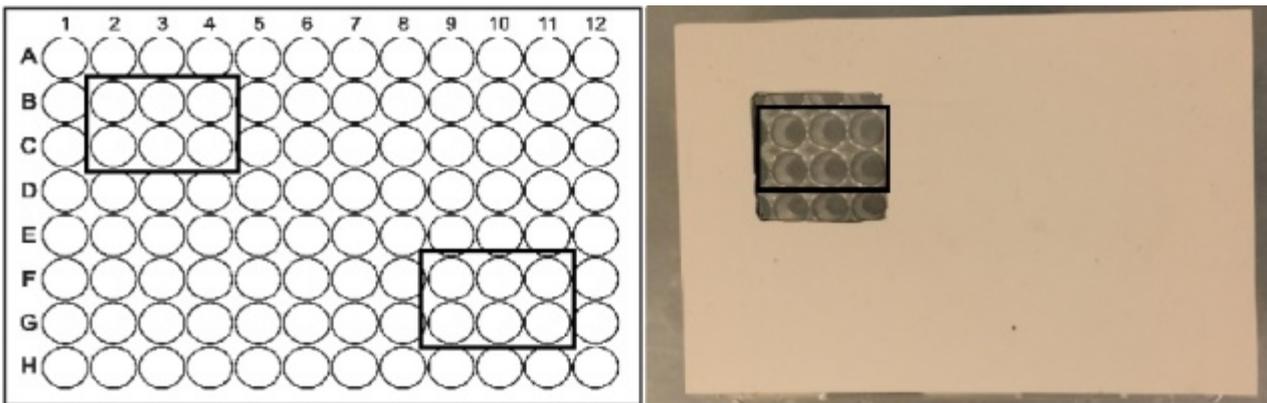

Figure 3. (Left) A template of a 96-well plate [32], the black boxes indicate the position of the wells containing hepes buffer. (Right) A 96-well plate with the customized lead-infused rubber placed on top. The black box indicates wells selected to be positioned in the primary radiation field.

The diameter of the circular applicator was 6 cm, the FSD varied between 15 and 22 cm, the irradiation angle varied between 0° and 30°. All parameters including the reduced field size were taken into account when the exposure time was calculated in order for the bottom of the wells to obtain an absorbed dose of 8 Gy. Analysis of the film samples was performed using the PTW-Verisoft v 3.2 software and Matlab.

3.2.2.3   *Dose profile*

In order to study the homogeneity of the dose profile and how it was influenced by the measurement depth a sample of film, the size of 7.0×7.0 cm^2, was placed on top of 2.2 cm PMMA and irradiated with a 100 kVp beam generated by an x-ray system (Gulmay D3100, Gulmay Medical). The obtained absorbed dose was 4.0 Gy, the FSD was 15 cm and a circular applicator with a diameter of 6 cm was used. The procedure was repeated with another sample of film, cut to the same size, however this time 8 mm PMMA was placed on top of the film before it was irradiated. A depth of 8 mm was selected as

the height of the wells of a 96-well plate was 8 mm and since some cells settle relatively fast, the dose profile at the maximum irradiation depth was investigated. The evaluation of the dose profiles were performed using the PTW-Verisoft v 3.2 software.

3.2.2.4 Confirm position of wells

When EBT3 dosimetry film is exposed to radiation it is blackened by the marker dye included in the active layer [30]. In order to compare the position of the exposed wells on the irradiated film, obtained by the PTW-Verisoft v. 3.2 software, with the actual position of the wells, a sample of film cut to the size of 10.2×14.0 cm^2 was placed on top of 3.0 cm PMMA. On top of the dosimetry film a 96-well plate, containing 50 µl hepes buffer in well B2-C4 and F9-G11, was placed. A customized lead-infused rubber with a 3.0×3.0 cm^2 hole was placed on top of the 96-well plate exposing well B2-C4, finally the position of the plate on the film was marked. The plate and film were irradiated perpendicular to the incident 100 kVp x-ray beam generated by a D3100 Gulmay (Gulmay Medical) and received an absorbed dose of 8 Gy. The outer diameter of a well in the 96-well plate was measured using a caliper and the inner diameter of the well was provided by the manufacturer. These diameters were compared with the mean inner and outer diameters obtained by measurements of 4 wells using the PTW-Verisoft v.3.2 software. As a further verification of the position of the 96-well plate the distance between the edge of the plate and one of the wells was measured and compared with the distance obtained from the markings and blackening on the film. This procedure was repeated once in order to verify the obtained results.

3.2.3 TLD

3.2.3.1 Calibration

In order to provide reference points for the measurements of unknown doses and to assure the instrument stability 12, 10 and 5 dosimeters were selected from the batch to be unknown, sensitivity and background calibration dosimeters respectively. To standardise their sensitivity and background level all dosimeters received a similar thermal treatment before exposure. The sensitivity dosimeters were placed on top of 3.0 cm PMMA, FSD was 15 cm, the diameter of the radiation field was 6 cm and the dosimeters were irradiated perpendicular to the incident 100 kVp beam generated by an x-ray system (Gulmay D3100, Gulmay Medical). The 10 sensitivity calibrations dosimeters were irradiated according to the manufacturer's specifications with a dose (0.1 Gy) very much greater than the expected standard deviation of the signal from the background calibration dosimeters.

3.2.3.2 Experiment

In order to verify the absorbed dose to the cells, 6 unknown dosimeters were placed in the positions of B2-C4 and the remaining 6 TLDs were placed in the F9-G11 positions of a 96-well plate. To simulate the radiation protocol 50 µl hepes buffer was added to each well containing a TLD dosimeter. The 96-well plate was placed on top of 3.0 cm PMMA and a customized lead-infused rubber, with a 3.0×3.0 cm^2 hole for the wells B2-C4, was placed on top of the plate. Using Sterling's equation [33], the equivalent field size for the 3.0×3.0 cm^2 radiation field was calculated and the distance from focus to the bottoms of the wells was measured to 16.8 cm. Both parameters were taken into account when the exposure time, to obtain an absorbed dose of 1.0 Gy at the bottoms of the wells, was calculated to 0.49 min. The 96-well plate placed on 3.0 cm PMMA was thereafter irradiated 0.49 min perpendicular to the incident 100 kVp beam generated by an x-ray system (Gulmay D3100, Gulmay Medical). The same procedure was applied when the absorbed dose to the cells placed on 25 cm ice and 2.2 cm PMMA was verified.

A Toledo TLD reader, model 654 (serial number 24-5), was used to read out the dosimeters one day after exposure, the standard heating cycle was used and the sensitivity and background settings were set as recommended by the manufacturer. All dosimeters, calibration and unknown were read out at the same occasion, unknown dosimeters interspersed with calibration dosimeters at regular intervals. The obtained absorbed dose, D, of an unknown dosimeter was calculated using

$$D = \frac{(x - B) \times C}{M - B},$$ (1)

where x was the read out of the unknown dosimeter, B the mean reading of the background dosimeters, C the absorbed dose of the sensitivity calibrations dosimeters and M the mean read out of the sensitivity dosimeters. Thereafter the mean absorbed dose to the TLDs placed in the primary radiation field (well B2-C4) was calculated, the same procedure was applied on the TLDs placed in the adjacent wells (F9-G11).

3.3   Results

3.3.1   GAFCHROMIC™ EBT3 film dosimetry

3.3.1.1   Calibration
The dose calibration curve obtained by PTW-FilmCal v. 2.3 is displayed in Figure 4, presenting the mean optical density (OD) as a function of the absorbed dose.
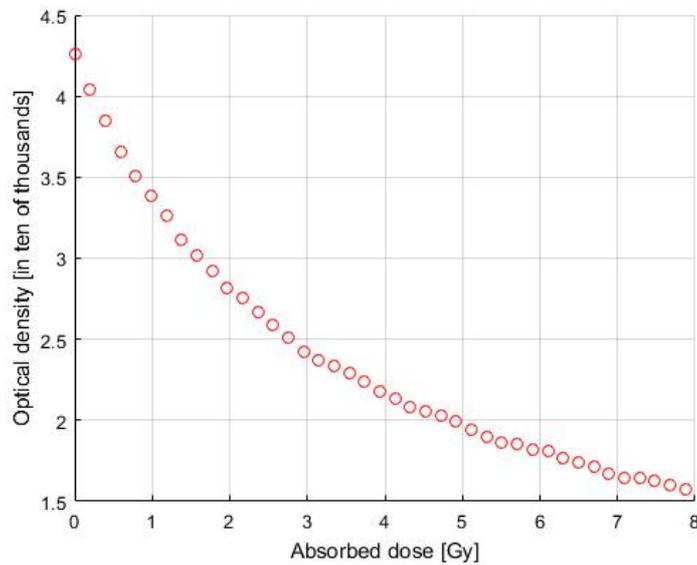

Figure 4. The generated calibration curve displaying the optical density in ten of thousands as a function of the absorbed dose.

The greatest relative standard deviation of the sample (RSD) obtained from the collected set of data during the calibration was 0.64%. In Figure 5 is the calculated RSD displayed for each sample of film.
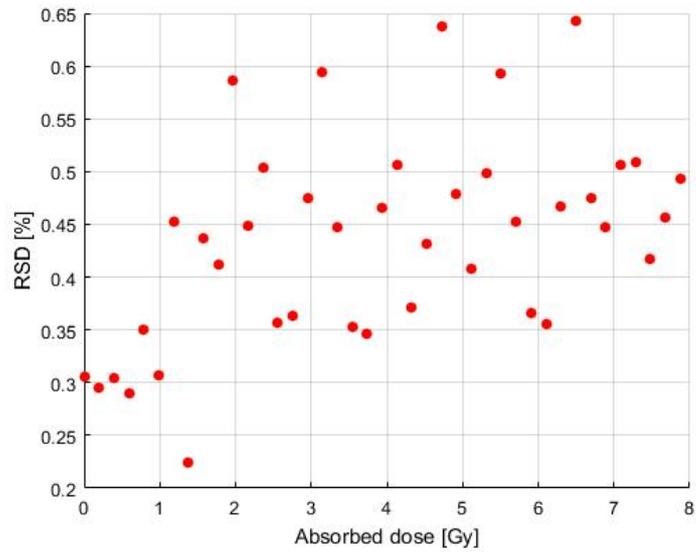
Figure 5. The obtained relative standard deviation (RSD) for each sample of film that were exposed to radiation during the calibration of the EBT3 dosimetry film.

3.3.1.2 Assessment of irradiation geometries

A line dose profile for the wells positioned in the primary radiation field for each one of the different irradiation geometries where the focus skin distance (FSD) was varied are displayed in Figure 6.
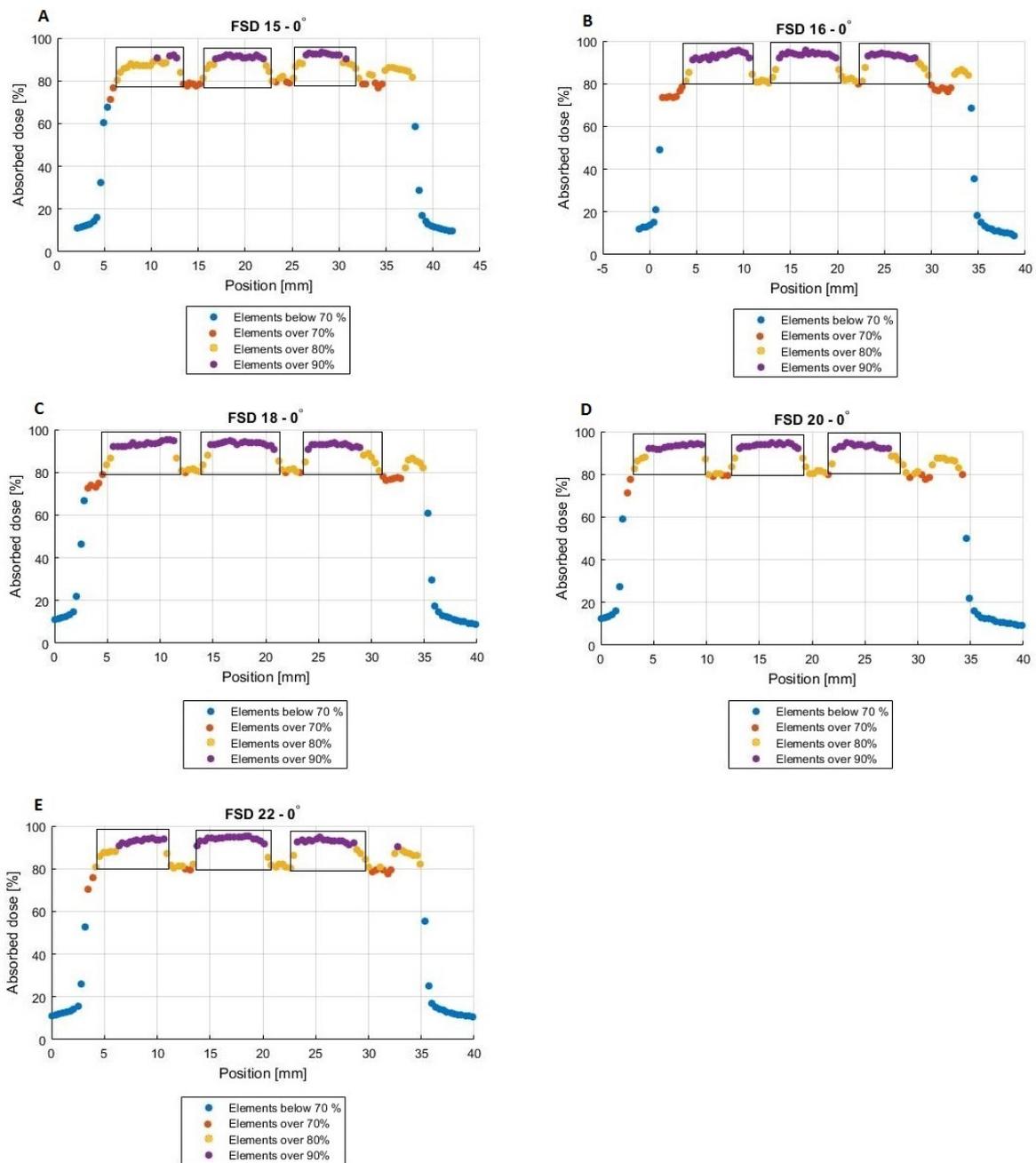
Figure 6. The dose profiles for the three wells positioned in the primary radiation field for the irradiation geometries where the focus skin distance (FSD) was varied. The black boxes indicate where the wells were positioned.

The dose profile of the irradiation geometries where the FSD was kept constant and the angle of irradiation varied is presented in Figure 7. As displayed in the aforementioned figure the angle of the x-ray tube is affecting the homogeneity of the dose delivery to the bottom of the wells and the positions of the wells are not as prominent as compared to the irradiations performed at an angel of 0°, compare Figure 6 and Figure 7.
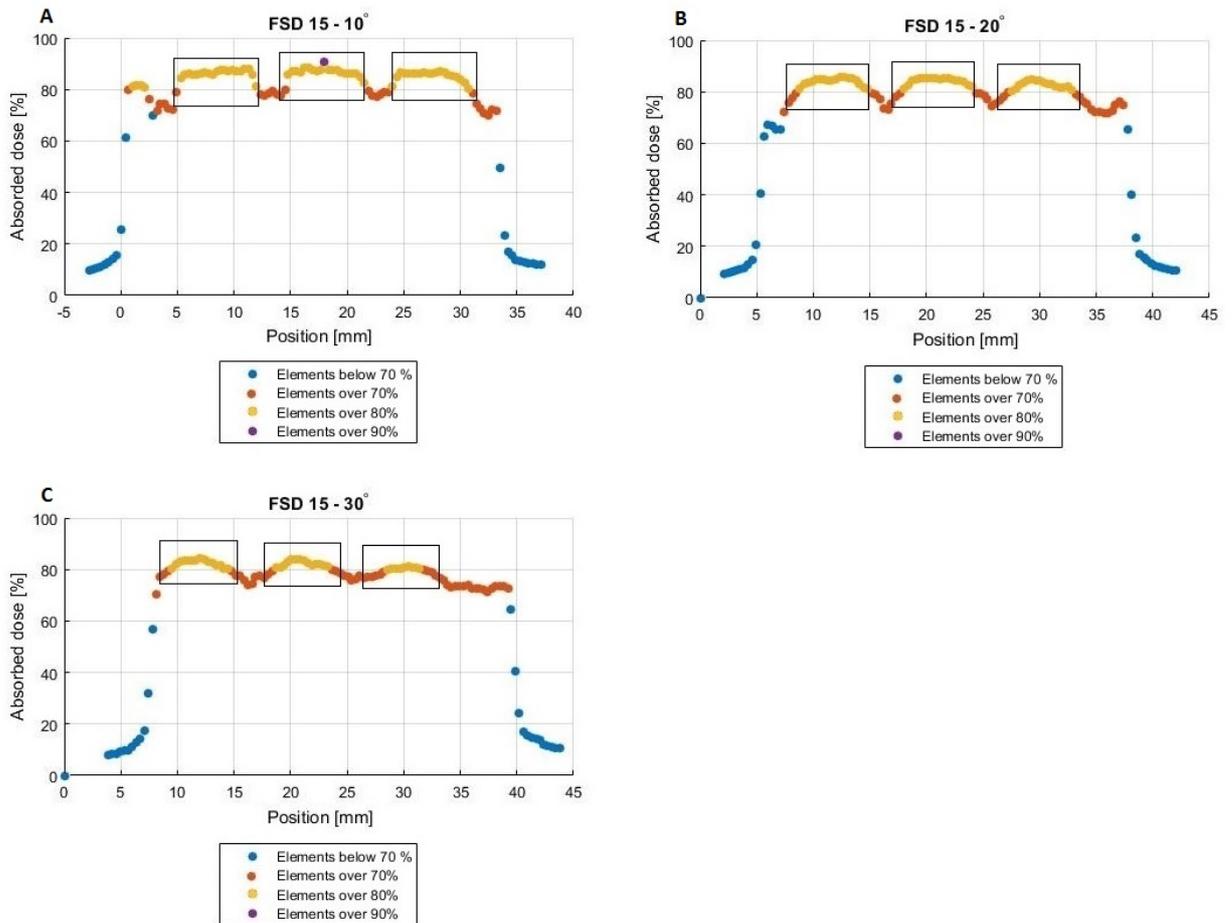
Figure 7. Dose profiles for the three wells positioned in the primary radiation field for the irradiation geometries were the angle of irradiation was varied. The black boxes indicate where the wells were positioned.

The mean (A_{Mean}^P), maximum (A_{Max}^P) and minimum (A_{Min}^P) delivered absorbed dose to the wells in the primary radiation field for the different irradiation geometries are displayed in Table 1.

Table 1. The mean, maximum and minimum absorbed dose obtained by the wells in the primary radiation field for the different irradiation geometries.

Irradiation geometry	A_{Mean}^P [Gy]	A_{Max}^P [Gy]	A_{Min}^P [Gy]
FSD 15 cm, angel of irradiation 0°	7.05±0.41	7.46	6.14
FSD 16 cm, angel of irradiation 0°	7.38±0.25	7.66	6.49
FSD 18 cm, angel of irradiation 0°	7.32±0.29	7.62	6.09
FSD 20 cm, angel of irradiation 0°	7.29±0.32	7.59	6.29
FSD 22 cm, angel of irradiation 0°	7.33±0.29	7.63	6.30
FSD 15 cm, angel of irradiation 10°	6.87±0.18	7.24	5.83

FSD 15 cm, angel of irradiation 20°	6.61±0.23	6.86	5.85
FSD 15 cm, angel of irradiation 30°	6.33±0.57	6.74	5.62

Regardless of the irradiation geometry the obtained mean (A_{Mean}), maximum (A_{Max}) and minimum (A_{Min}) absorbed dose to the wells not positioned in the primary radiation field were significantly lower than the measured absorbed dose to the wells in the radiation field (see Table 2).

Table 2. The mean, maximum and minimum absorbed dose obtained by the wells adjacent to the primary radiation field for the different irradiation geometries.

Irradiation geometry	A_{Mean} [Gy]	A_{Max} [Gy]	A_{Min} [Gy]
FSD 15 cm, angel of irradiation 0°	0.05±0.02	0.14	0
FSD 16 cm, angel of irradiation 0°	0.05±0.2	0.08	0
FSD 18 cm, angel of irradiation 0°	0.03±0.02	0.07	0
FSD 20 cm, angel of irradiation 0°	0.05±0.02	0.10	0
FSD 22 cm, angel of irradiation 0°	0.05±0.02	0.11	0
FSD 15 cm, angel of irradiation 10°	0.03±0.02	0.06	0
FSD 15 cm, angel of irradiation 20°	0.03±0.02	0.08	0
FSD 15 cm, angel of irradiation 30°	0.03±0.02	0.06	0

3.3.1.3   Dose profile

As seen in Figure 8 is the absorbed dose to target dependent on the position in the radiation field when the measurement was performed at the surface. The diameter of the circular radiation field was 6.0 cm and great variations in the delivered absorbed dose were obtained (see Figure 8 and Table 3). However the elements obtaining the lowest absorbed doses were placed at the edge of the radiation field. The mean delivered absorbed dose to target, for the inner circle of the radiation field with a diameter of 3.0 cm, 4.0 cm and 6.0 cm, is displayed in Table 3 along with the values for the maximum and minimum absorbed dose.
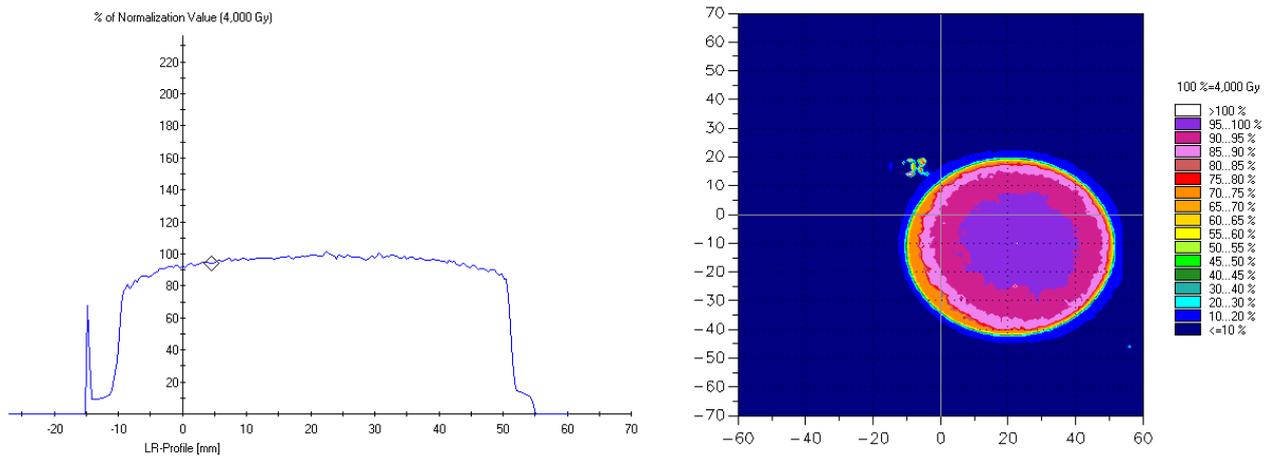
Figure 8. (Left) The dose profile obtained at the surface displaying the absorbed dose in percent as a function of the position of the radiation field. (Right) Isodose of the radiation field obtained at the surface. The tonality to the right indicates that the colour blue corresponds to absorbed doses in the range of 0-30 % and that purple and pink corresponds to absorbed doses in the range of 85-100%.

The dose profile and isodose for the measurement performed at a depth of 8 mm are presented in Figure 9.
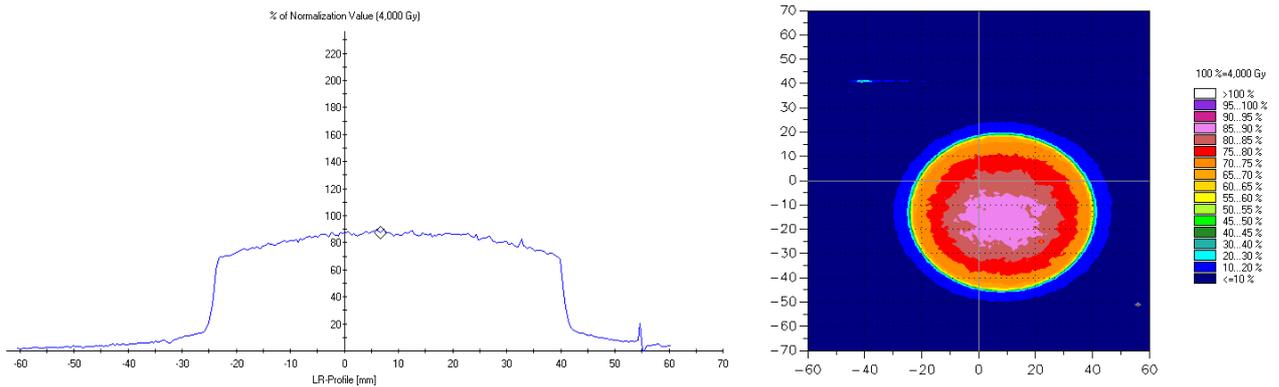

Figure 9. (Left) The dose profile obtained at 8 mm depth displaying the absorbed dose in percent as a function of the position of the radiation field. (Right) Isodose of the radiation field obtained at 8 mm depth. The tonality to the right indicates that the colour blue corresponds to absorbed doses in the range of 0-30 % and that purple and pink corresponds to absorbed doses in the range of 85-100%.

The maximum delivered absorbed dose to target was lowered by approximately 10% (see Figure 9 and Table 3) when 8 mm PMMA were placed on top of the film. Large variations in the absorbed dose within the circular radiation field with a diameter of 6.0 cm were still obtained; however the elements obtaining the lowest absorbed dose were still located at the edge of the radiation field. The mean delivered absorbed dose to target, for the inner circle of the radiation field with a diameter of 3.0 cm, 4 cm and 6 cm, is displayed in Table 3 along with the maximum and minimum absorbed dose.

Table 3. The measured mean, maximum and minimum absorbed dose for a circular radiation field with a diameter of 3 cm, 4 cm, and 6 cm, at the surface and on 8 mm depth.

	Diameter radiation field [cm]	A_{mean} [Gy]	A_{max} [Gy]	A_{min} [Gy]
Surface	3	3.92±0.05	4.05	3.76

	4	3.89±0.07	4.05	3.67
	6	3.78±0.25	4.05	1.97
	3	3.46±0.05	3.60	3.34
8 mm depth	4	3.42±0.09	3.60	3.17
	6	3.30±0.20	3.60	2.81

3.3.1.4 Confirm position of wells

Using the software PTW-Verisoft v.3.2 the inner and outer diameter of 8 wells of a 96-well plate were determined, see Figure 10.
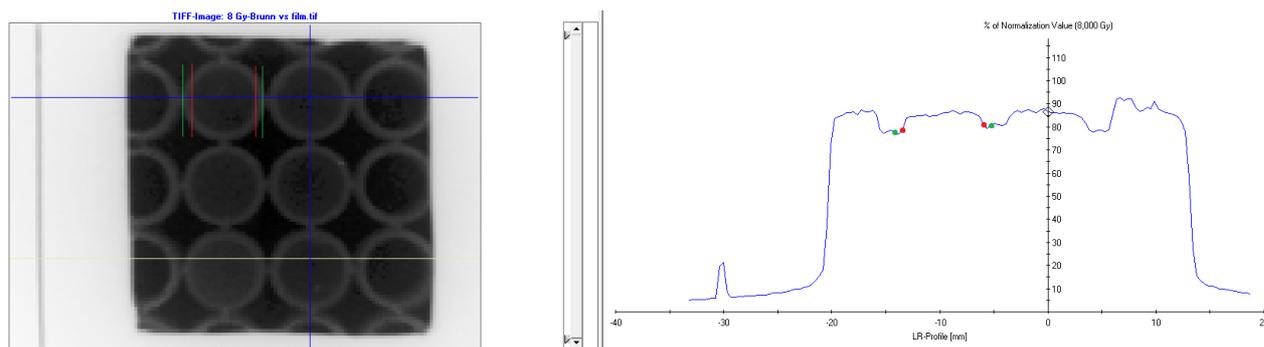

Figure 10. The figure displays the PTW-Verisoft v. 3.2 panel. (Left) Image of the scanned dosimetry film, displaying the wells positioned in the primary radiation field. (Right) Left-Right dose profile of the wells that displays the absorbed dose in percent as a function of the position. The red and green markers, placed by the observer, representing the inner and outer diameter respectively.

The mean inner and outer diameters of the wells were calculated using the PTW-Verisoft v.3.2 software and compared with the diameters measured by a calliper or obtained by the manufacturer, the result is displayed in Table 4. Regarding the determination of the distance between the edge of the 96-well plate and one of the wells the two methods of measurements displayed no discrepancies.

Table 4. The table displays the inner and outer diameter of a well on a 96-well plate obtained by measurements performed with a caliper or obtained by the manufacturer and the software PTW-Verisoft v. 3.2.

	Inner diameter [mm]	Outer diameter [mm]
Obtained by manuf./Measured	6.8	8.4
GAFCHROMIC^{TM} EBT3 Dosimetry Film	6.9 ± 0.2	8.4 ± 0.1

3.3.2 TLD

To further confirm the absorbed dose to the cells, TLDs placed in the selected wells of a 96-well plate were irradiated according to the two irradiation geometries, see section *4.2.2.2 Irradiation with Gulmay D3100*. The mean absorbed dose, *A*, to the TLDs placed in the primary radiation field and to TLDs in the adjacent wells (wells B2-C4 and F9-G11 respectively) was calculated using equation (**1** and the result is displayed in Table 5.

Table 5. The mean absorbed dose to the wells (B2-C4) in the primary radiation field and to the adjacent wells (F9-G11) that were not placed in the primary radiation field.

	A_{B2-C4} [Gy]	A_{F9-G11} [Gy]
37°C irradiation geometry	0.97 ± 0.06	0.01 ± 0.004
5°C irradiation geometry	0.97 ± 0.02	0.02 ± 0.004

3.4   Discussion

3.4.1   GAFCHROMIC™ EBT3 Dosimetry film

3.4.1.1   Calibration

The greatest obtained relative standard deviation (RSD), during the calibration of the dosimetry film was 0.64%. It was assumed that the dose delivery in the defined region of interest was homogeneous and it is therefore possible to state that the intrinsic film inhomogeneity corresponds to the maximum obtained value of the RSD. This suggests that the intrinsic film inhomogeneity is less than the uncertainty for EBT film recommended by van Battum et al [31]. However the author is aware that the underlying assumption does not correspond to the reality, as the dose delivery in the specified region of interest was not homogeneous, see Table 3 in section *3.3.1.3 Dose profile*. As a result the uncertainty in the dose delivery will be underestimated if an uncertainty of 0.64% is applied. However, other uncertainties are introduced in the measurements, e.g. the scanner, fit accuracy of generated calibration curve and energy dependence of the film. These sources introduce minor uncertainties and using recommendations and data published by Borca et al. [30], the overall uncertainty in EBT3 film dose detection is estimated to be no less than 1.7%.

3.4.1.2   Assessment of different irradiation geometries

As can be determined from Figure 6 A-E and Table 1, the variations in the delivered absorbed dose to the wells in the primary radiation field are reduced when the focus skin distance (FSD) is increased, this may be due to the inverse-quadratic law. A difference in the distance between a well positioned straight underneath the source and a well positioned closer to the edge of the divergent radiation field will be less significant the greater the FSD is. However, owing to technical difficulties a FSD greater than 15 cm was difficult to ensure and since the experiment was to be repeated several times it was considered more important to ensure the reproducibility of the irradiation geometry. It was therefore decided that a FSD of 15 cm and an angle of 0° were to be the irradiation geometry throughout the study, even though this decision resulted in a somewhat greater absorbed dose to the wells not placed in the primary radiation field (see Table 2). From Figure 6 and Figure 7, it can be concluded that in order to reduce the inhomogeneity in the delivered absorbed dose to the bottom of the wells the angle of irradiation should be 0°. Otherwise the FSD to the exposed wells will differ, resulting in an inhomogeneous dose distribution to the exposed wells due to the inverse-quadratic law (e.g see Figure 7 C). As a result of the need for the radiation to pass through the walls of the wells when irradiating at an angle, the absorbed dose to the bottom of the wells will be reduce further. Thus the delivered absorbed dose to the wells in the primary radiation field and to the adjacent wells is lowered when irradiating at an angle (see Table 1 and Table 2).

In Table 2 the maximum and mean absorbed dose to the wells in the primary radiation field was somewhat lower than expected, even though the different FSD and angles of irradiation was accounted for. This may be due to the fact that the radiation penetrated the lid of the 96-well plate and the bottom of the well before encountering the dosimetry film. The thickness of the lid and bottom of the well were 0.9 mm and 3.2 mm PMMA respectively. To correct for the thickness of the bottoms of the wells the depth dose curve for the x-ray system (see Appendix 1) for 100 kVp was used. Using the depth dose curve the absorbed dose for the selected irradiation geometry to the wells in the primary radiation field (B2-C4) and to the adjacent wells (F9-G11) was corrected, see Table 6.

Table 6. The table presents the corrected obtained absorbed dose to the wells placed in the primary radiation field and the adjacent wells at a focus skin distance (FSD) of 15 cm and with an angel of irradiation of 0°.

Wells	A_{Mean} [Gy]	A_{Max} [Gy]	A_{Min} [Gy]
B2-C4	7.69 ± 0.29	8.06	6.64
F9-G11	0.05 ± 0.03	0.15	0

From Table 6, it can be concluded that the obtained absorbed dose to the bottom of the wells was still less than 8 Gy and this may depend on the intrinsic fluctuations of the x-ray system generating the 100 kVp beam. Discrepancies in the measured and the anticipated absorbed dose may also be due to the fact that x-rays passed through the lid of the 96-well plate, consisting of 0.9 mm PMMA, before reaching the bottom of the wells or due to the uncertainty of the film measurements. The uncertainty in dose detection using the EBT3 dosimetry film was estimated to 1.7%. By applying this estimated uncertainty to the corrected values of the absorbed dose in Table 6 it is assumed that the measured absorbed dose corresponds to the anticipated and that the dose delivery to the wells is assured. As can also be concluded from Table 6, the delivered absorbed dose to the adjacent wells (F9-G11) is approximately 1% of the delivered dose to the wells located in the primary radiation field. The dose contribution to the adjacent wells was therefore disregarded.

3.4.1.3   Dose profile

As can be concluded from Figure 8 and Table 3 variations within the radiation field at the surface are obtained. The greatest difference in the delivered absorbed dose is 2.1 Gy for the radiation field with a diameter of 6.0 cm, however the mean absorbed dose for the mentioned radiation field size is 3.78 ± 0.25. It is therefore assumed that the elements obtaining an absorbed dose close to the minimum dose (1.97 Gy) are few and located close to the edge of the radiation field. With regard to Figure 8, this assumption be can verified. It is also noted that the inhomogeneity in the delivery of the absorbed dose was reduced for the inner radiation field with a diameter of 3.0 cm and 4.0 cm.

The variations in the delivered absorbed dose may be due to the divergent radiation field, resulting in a small difference in distance between focus and an element directly underneath focus compared with the distance between focus and an element at the edge of the radiation field. Intrinsic variations of the generation of 100 kVp beam in the x-ray system may also contribute to the inhomogeneous dose delivery. The obtained asymmetric dose profile at the surface could be a result of the x-ray tube being placed at a small angle on top of the film sample during the irradiation. This is considered likely as the dose profile at 8 mm depth was symmetric, see Figure 9. In order to minimize the effect of the inhomogeneous dose delivery the positioning of the exposed wells in the 96-well plate was performed with care, thus ensuring that they were always placed within the inner circle of the radiation field with a diameter of 4.0 cm.

As expected was the delivered absorbed dose at the depth of 8 mm PMMA lower than the obtained absorbed dose at the surface, see Table 3. The measured absorbed dose at the depth of 8 mm PMMA corresponds to a dose response of 84% (see depth dose curve in Appendix 1). For the radiation fields with a diameter of 3.0 cm, 4.0 cm, and 6.0 cm the measured mean absorbed dose at 8 mm depth corresponded to 88%, 88%, and 87% of the mean dose to the surface, respectively. The inconsistency may be caused by intrinsic variations in the generation of the 100 kVp beam by the x-ray system and/or by intrinsic film inhomogeneity.

The variations within the radiation field at a depth of 8 mm, regardless of size, are consistent with the variations found at the dose delivery at the surface, nonetheless is the greatest difference in the dose

delivery somewhat reduced. This may be due to a beam hardening effect since x-rays have passed through 8 mm of PMMA before encountering the dosimetry film.

3.4.1.4 Confirm position of wells

It can be concluded from Table 4 that a small to none discrepancy between the two methods of measurement were found when determining the inner and outer diameter of the wells. No difference in the distance between the edge of the 96-well plate and one of the wells were found using the two methods of measurements and only a small to none discrepancy was found when determining the inner and outer diameter of the wells. It is therefore assumed that the position of the wells in the dosimetry film corresponds to the actual position of the wells and it is probable that the obtained discrepancies are caused by inconsistency in the observer's determination of the edge of the wells. Another element that may have contributed to the discrepancies between the two methods of measurements is if the films were slightly askew while they were scanned. The PTW-Verisoft 3.2 software can only determine the distance in direct horizontal and vertical line and cannot compensate for skewness. However, the inconsistency of the observer in determining the inner and outer edge of the wells using the PTW-Verisoft v. 3.2 software is considered the most probable reason for obtaining inconsistencies between the two methods of measurements.

3.4.2 TLD

As is displayed in Table 5, the obtained mean delivered absorbed dose to wells in the primary radiation field (wells B2-C4) is close to the expected absorbed dose of 1 Gy regardless of the irradiation geometry. Why the measured absorbed dose does not fully comply with the expected absorbed dose of 1 Gy may be that the x-rays have penetrated the lid of the 96-well plate before reaching the TLDs. Using the depth dose curve of the x-ray system (see appendix 1) an obtained absorbed dose at a depth of 0.9 mm in PMMA corresponds to a 96% dose response. This corresponds to the obtained result when the uncertainties for respective irradiation geometry are considered. From Table 5, it is concluded that the uncertainty, i.e. the standard deviation of the sample, is somewhat greater for the 37°C irradiation geometry than the 5°C irradiation geometry. This may be due to reduced back scatter at the 5°C irradiation geometry, owing to the increase thickness of low Z-materials underneath the 96-well plate. To summarize, the obtained absorbed dose for both irradiation geometries displays a little to no discrepancy to the expected value of 1 Gy and it is therefore assumed that the anticipated absorbed dose to the bottom of the wells corresponds with the actual dose delivery.

The obtained absorbed dose to the adjacent wells not positioned in the primary radiation field is 1% and 2% of the expected delivered absorbed dose to the exposed wells, see Table 5. Since the greatest delivered absorbed dose to the wells in the primary radiation field is 16 Gy the largest dose contribution to the cells positioned in the adjacent wells will be 0.32 Gy. It is thus concluded that the dose contribution to the adjacent well can be neglected.

3.5 Conclusion

Two optimal irradiation geometries ensuring the dose delivery to the wells positioned in the primary radiation field and contributing with a negligible small dose contribution to the adjacent wells were found. Measurements using EBT3 dosimetry film and TLDs confirmed that the delivered absorbed dose to the wells of a 96-well plate in the two irradiation geometries used in this study corresponded to the expected absorbed dose. It is therefore concluded that the absorbed dose for conditions relevant for studies of the concurrent effect of radiation and calcium was assured in this study.

4. Studies of cell viability

4.1   Aims and Hypotheses

In this part of the project the hypothesis is that by combining radiation and calcium the influx of calcium through the permeabilized cell membrane will increase, resulting in energy depletion and cell death. Following this hypothesis the concurrent effect of radiation and calcium would manifest as reduced cell viability. Aims of this study are to

- Investigate the survival of two cancer cell lines exposed to high levels of calcium in combination with radiation,
- Study if the potential effect of calcium on the survival fraction is influenced by the absorbed dose.

4.2   Materials and Methods

4.2.1   Preparations

4.2.1.1   Cell culturing

The SW780 human bladder transitional cell carcinoma cell line was kindly provided by Dr. Lars Dyrskjøt Andersen, Department of Molecular Medicine, Aarhus University Hospital, Skejby, Denmark and the and H69 human small-cell lung cancer cell line was kindly provided by the Department of Oncology, Copenhagen University Hospital, Denmark. The cell lines were maintained in RPMI 1640 culture medium containing 10 % foetal calf serum, 100 U/ml penicillin and 100 μg/ml streptomycin and kept at 37°C and 5 % CO_2.

4.2.1.2   Preparation MTS assay

SW780 cells were harvested using trypsinization. First the medium was removed and the cells were rinsed with a phosphate-buffered saline (PBS), thereafter trypsin was added and the cell suspension was incubated at 37°C for a couple of minutes until the cells loosened from the cell culture flask. Next, cell culture medium was added to the re-suspended cells and transferred into a tube.

The H69 cells are growing as spherical floating aggregates and were thus harvested by using a scrape at the bottom of the cell culture flask; afterwards cells and the cell culture medium were transferred into a tube.

The tubes of both cell lines were centrifuged and the medium was removed. Both cell lines were washed with hepes buffer (containing 10 mmol/L hepes (Lonza), 250 mmol/L sucrose, and 1 mmol/L $MgCl_2$ in sterile water), centrifuged again, new hepes was added to the tubes and the cell suspensions were diluted into the desired concentration (600,000 cells/ml). The cell suspensions for SW780 and H69 were each divided into two sets of tubes where 5 mM $CaCl_2$ (final concentration) was added into one of the tubes of each cell line. *This is to be compared with the intracellular calcium concentration of ~0.1 mM in normal cells [15].* Finally, 50 μl from each suspension was transferred into 6 wells (B2-C4 or F9-G11) of a 96-well plate.

When the irradiation was performed in the 5°C geometry (see section *4.2.2.2 Irradiation with Gulmay D3100*) the aforementioned preparation of the cell suspension was performed on ice.

4.2.1.3   Preparation Clonogenic assay

One day before treatment the SW780 cell suspension in cell culture medium was diluted to the desired seeding concentrations (20, 100 and 200 cells/ml) and 5 ml of each suspension was seeded in four wells of a 6-well plate and incubated overnight at 37 °C and 5% CO_2. This procedure was repeated three times, resulting in a total of six 6-well plates.

At the day of treatment the cell culture medium was removed and replaced with 5 ml hepes buffer with or without 5 mM calcium.

4.2.2   Radiation protocol

4.2.2.1   Controls

In order to investigate how incubation time after irradiation and the irradiation procedure affected the cell survival rate, cell suspensions, diluted in hepes buffer and in cell culturing medium, were prepared and plated in the 96-well plates according to the aforementioned procedure. For each cell line one 96-well plate containing cells diluted in hepes buffer and medium was placed in the incubator at 37°C and 5% CO_2. Another 96-well plate transported to the place of irradiation was kept at the same conditions as the plates that were irradiated, i.e. kept at a temperature close to 37°C. The temperature of the cells was maintained by keeping the plates in an insulating box interspersed with heating blocks containing water with a temperature of 37°C. Plates were only removed and exposed to room temperature during the irradiation. This assured that the temperature was as close to 37°C during the experiment as was reasonable achievable and the temperature of the cells in the transportation box and at the location of irradiation is from now on referred to as 37°C in this study. When the irradiation of the 96-well plates of each cell line containing cells diluted in hepes buffer was complete (procedure described in section *4.2.2.2 Irradiation with Gulmay D3100*) all plates were incubated at 37°C and 5% CO_2 for one day (21 hours) or two days (46 hours). The cells viability was assessed using the procedure mentioned in section *4.2.3 MTS viability assay*.

To evaluate the impact of changes in temperature, occurring when the cells were irradiated at the 5°C irradiation geometry, the above mentioned procedure was repeated for the 5°C irradiation geometry. Cells were transported and kept on ice during the experiment. The viability of the cells irradiated at 5°C was only evaluated after two days of incubation at 37°C and 5% CO_2.

Result from experiments using 37°C irradiation geometry is displayed on a white background while results from experiments using 5°C irradiation geometry is displayed on a grey background.

4.2.2.2   Irradiation with Gulmay D3100

A customized lead-infused rubber with a 3.0×3.0 cm^2 hole was placed on top of a 96-well plate, exposing the selected wells (well B2-C4 or F9-G11), see Figure 3.

The 96-well plate was placed on 3.0 cm polymethylmethacrylate (PMMA) (referred to as the "37°C irradiation geometry") or on 2.2 PMMA and 25 cm ice (referred to as the "5°C irradiation geometry") perpendicular to the incident 100 kVp beam generated by an x-ray-system (Gulmay D3100, Gulmay Medical). Figure 11 displays the 37°C irradiation geometry (A) and the 5°C irradiation geometry (B).
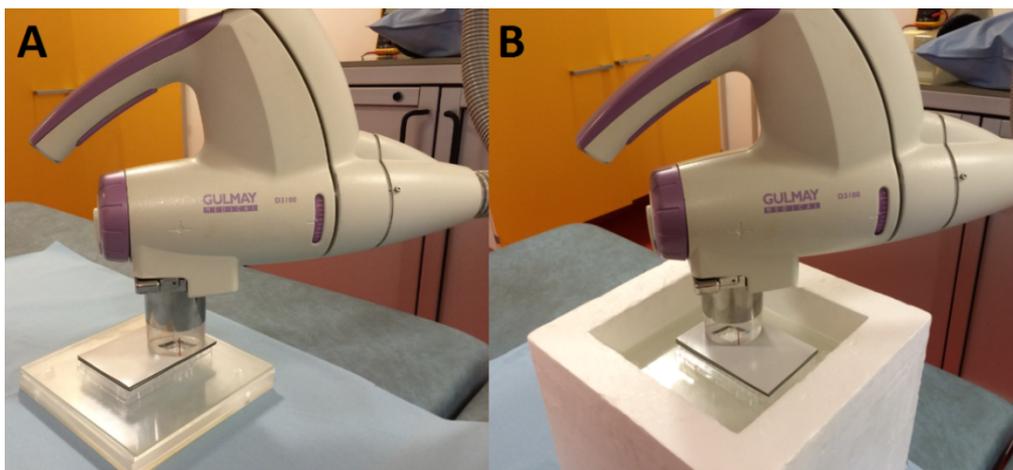
Figure 11. The 37°C irradiation geometry (A) and the 5°C irradiation geometry (B).

The focus skin distance (FSD) was 15.0 cm and the diameter of the circular radiation field was 6 cm. Plates were irradiated to obtain an absorbed dose of 0, 2, 4, 8, or 16 Gy, respectively. During the transportation and at the location of irradiation, plates that were to be irradiated in the 37°C or 5°C irradiation geometry were kept at the corresponding temperature. This procedure was performed for each cell line, including cells treated with and without calcium, and repeated four times.

In order to study if the MTS assay registered the dose-response of the cells one exposure of the SW780 cell line, where an absorbed dose of 100 Gy was delivered and the 96-well plate was placed according to the 5°C irradiation geometry, was performed.

4.2.2.3 Irradiation with Varian IX

In order to confirm the results obtained by MTS assay from the irradiation with 100 Gy using the x-ray system (D3100 Gulmay, Gulmay Medical) and to confirm the dose delivery of the x-ray system one experiment exposing SW780 cells to 100 Gy was performed on a Varian 2300iX Clinic linear accelerator (Varian Medical Systems, Inc., Palo Alto, CA). The Varian 2300iX Clinic linear accelerator (Varian Medical Systems, Inc., Palo Alto, CA) was also used to study if it was possible to detect the dose-response of irradiated cells using MTS assay and compared this with the golden standard, clonogenic assay. A linear accelerator was preferably used as the time of irradiation was drastically shortened and by using another source of radiation the dose delivery of the x-ray system could be verified. The field size was 15.0×15.0 cm^2, the energy was 6 MV, the plates containing SW780 cells were placed perpendicular to the incident beam on top of 3 mm PMMA and 25 cm ice and water at isocenter (SSD=100 cm) with 6.9 cm of PMMA above the plates, see Figure 12.
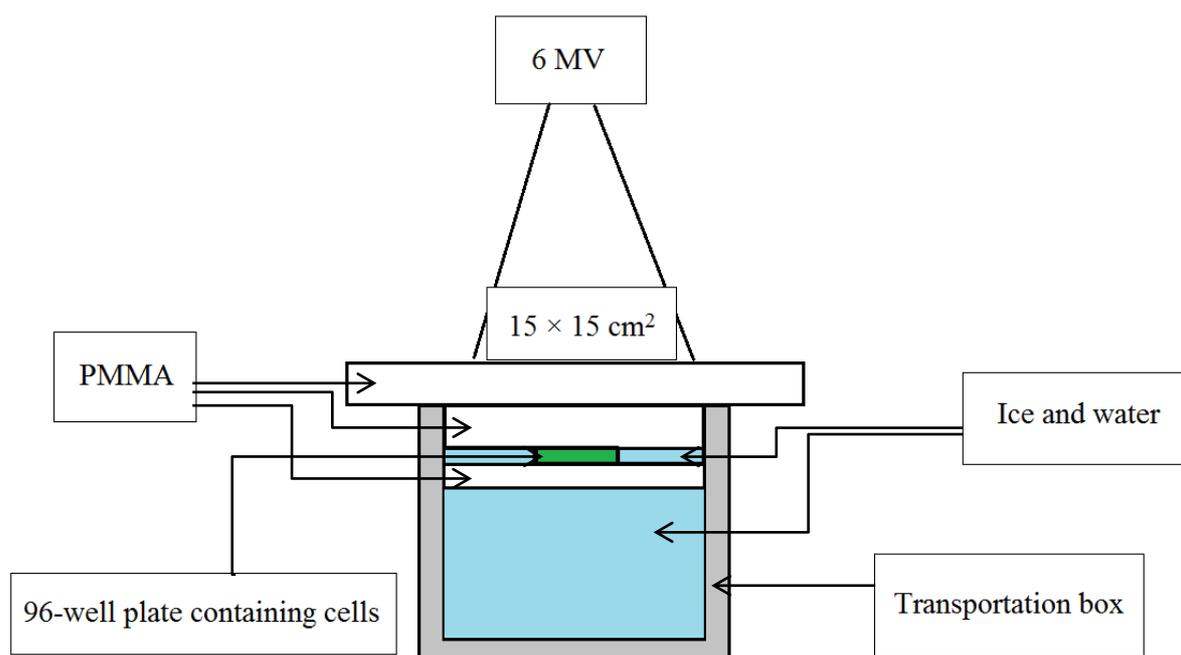
Figure 12. The irradiation geometry used when irradiating a 96-well plate or three 6-well plates using a Varian 2300iIX Clinic linear accelerator (Varian Medical Systems, Inc., Palo Alto, CA).

The absorbed dose at isocenter was calculated to 0.895 Gy/100 MU using Eclipse with a maximum lateral dose fluctuation of 0.8%. One 96-well plate containing SW780 cells treated with and without calcium was exposed to an absorbed dose of 100 Gy. Three 6-well plates, containing SW780 cells treated with and without calcium, were irradiated in the irradiation geometry described in Figure 12 and obtained an absorbed dose of 4 Gy.

4.2.3   MTS viability assay

The viability of SW780 and H69 cells, treated with or without calcium and/or radiation, were evaluated using MTS viability assay. After treatment 150 µl culture medium was added to each well and the 96-well plates were placed in an incubator (37°C and 5 % CO_2) for two days (43-46 hours), thereafter 40 µl MTS was added to each well. The cell viability was assessed after 1-1.5 hours of incubation at 37°C and 5 % CO_2 by measuring the optical density (OD) using a Synergy HT BIO-TEK reader at 492 nm and background measurements at 590 nm.

4.2.3.1   *Statistical analysis*

The Shapiro-Wilk test was used to determine if the collected set of samples were normally distributed and a qq-plot was used to investigate the distribution of the collected sample data. Differences in survival between groups were evaluated using a 2-way ANOVA (Analysis of Variance) with Bonferroni correction and the statistical analysis was performed using SAS 9.2 software (SAS Institute Inc.). If the obtained p-value was less than 0.05 the null hypothesis (that the population was normally distributed or that there was no difference in survival between the groups) was to be rejected.

4.2.4 Clonogenic assay

To study the effect of radiation an in vitro cell survival assay was performed. After exposing three 6-well plates with cells treated with and without calcium to an absorbed dose of 4 Gy a total of 3 ml of hepes buffer was removed from the wells and 5 ml RPMI 1640 culture medium was added to each well. Thereafter the 6-well plates were placed in an incubator (37°C and 5% CO_2). The same procedure, excluding the irradiation, was performed on the remaining three 6-well plates containing cells treated with and without calcium.

A week after treatment the medium was removed and the plates were rinsed with PBS. The PBS was removed and 2-3 ml of a mixture of 6 % of ethanol and 0.5% crystal violet was added to each well. After 1 hour the mixture was carefully removed and the plates were rinsed with distilled water, thereafter the plates were left to dry in normal air at room temperature.

When combination treatments are carried out, e.g. drugs in combination with ionizing radiation, surviving fractions as a function of dose can be determined by using clonogenic assay. However, the proliferation rate might be influenced by the drug, in this study calcium, and the colony formation might take a longer period of time than for radiation alone. This combination of treatments may affect the radiation dose-survival curve, yielding a result expressed as a dose enhancement ratio (*DER*)

$$DER = \frac{Dose\ with\ radiation\ alone}{Dose\ with\ radiation + Drug} \text{ for the same biological effect.} \qquad (2)$$

If the DER is greater than 1 the drug functions as a radiosensitiser and if the DER is less than 1 the drug is a radioprotector. However, due to the lack of time, a radiation dose-survival curve could not be obtained in this study. It was therefore decided that plating efficiency (*PE)* and survival fraction (*SF*) for cells treated with calcium should be calculated following the standard procedure applied for cells treated without calcium.

Using equation 3 the plating efficiency for cells treated with and without calcium was determined

$$PE = \frac{no.of\ colonies\ formed}{no.of\ cells\ seeded} \times 100\%. \qquad (3)$$

The number of colonies formed after radiotherapy was counted and the survival fraction (*SF)* of the irradiated cells, expressed in terms of *PE*, was calculated using

$$SF = \frac{no.of\ colonies\ formed\ after\ treatment}{no.of\ cells\ seeded \times PE/100}. \qquad (4)$$

The obtained *SF* was compared with the estimated survival rate. Estimation of the expected survival was based on the linear-quadratic model and α- and β-values for bladder cancer cells were collected from literature [34]. The fraction of cells surviving (*S*) an absorbed dose of 4 Gy (*D*) was thereafter calculated using

$$S = e^{-\alpha D - \beta D^2}. \qquad (5)$$

4.3 Results

4.3.1 Controls

4.3.1.1 *Controls of the 37°C irradiation geometry*

Presented in Figure 13 and Figure 14 are the survival of cells diluted in cell culture medium and hepes buffer that was incubated for one day (21 hours) and two days (46 hours) for the SW780 and H69 cell line respectively. The obtained survival fraction (SF) for both cell lines was normalized to the cells suspended in cell culture medium and incubated at 37°C.
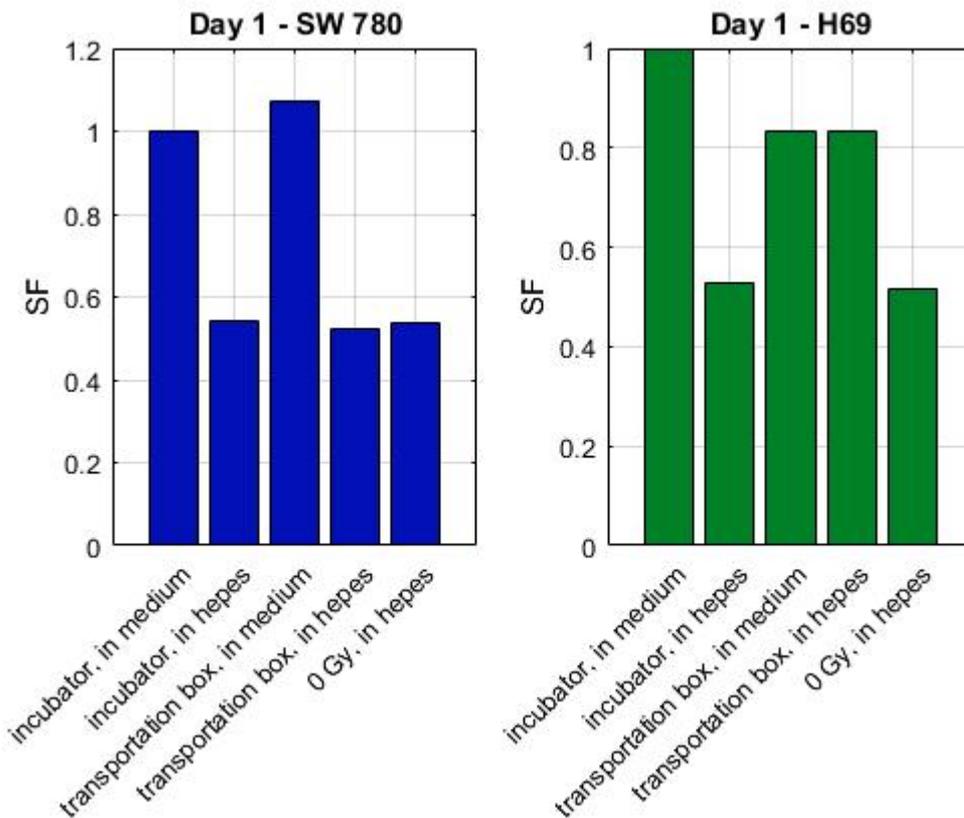

Figure 13. The measured survival fraction (SF) of SW780 and H69 cells are displayed to the left and right respectively (n=1) after one day of incubation at 37°C and 5% CO_2 after treatment. Results have been normalized to the survival obtained by cells diluted in cell culture medium and incubated at 37°C. Cells were diluted in cell culture medium ('incubator, in medium') or hepes buffer ('incubator, in hepes') and placed in an incubator at 37°C and 5% CO_2 corresponding to the time it took to transport the plates to the place of irradiation and irradiated them with 0×2, 2×2, 4×2 and 8×2 Gy in the 37°C irradiation geometry. Cells were diluted in cell culture medium ('transportation box, in medium') or hepes buffer ('transportation box, in hepes') and transported to the location of irradiation and kept in an isolated transportation box with 37°C heating blocks for the time corresponding to irradiation of 0×2, 2×2, 4×2 and 8×2 Gy in the 37°C irradiation geometry. Cells were diluted in hepes buffer and placed under the x-ray system without any applied absorbed dose ('0 Gy, in hepes') in the 37°C irradiation geometry.
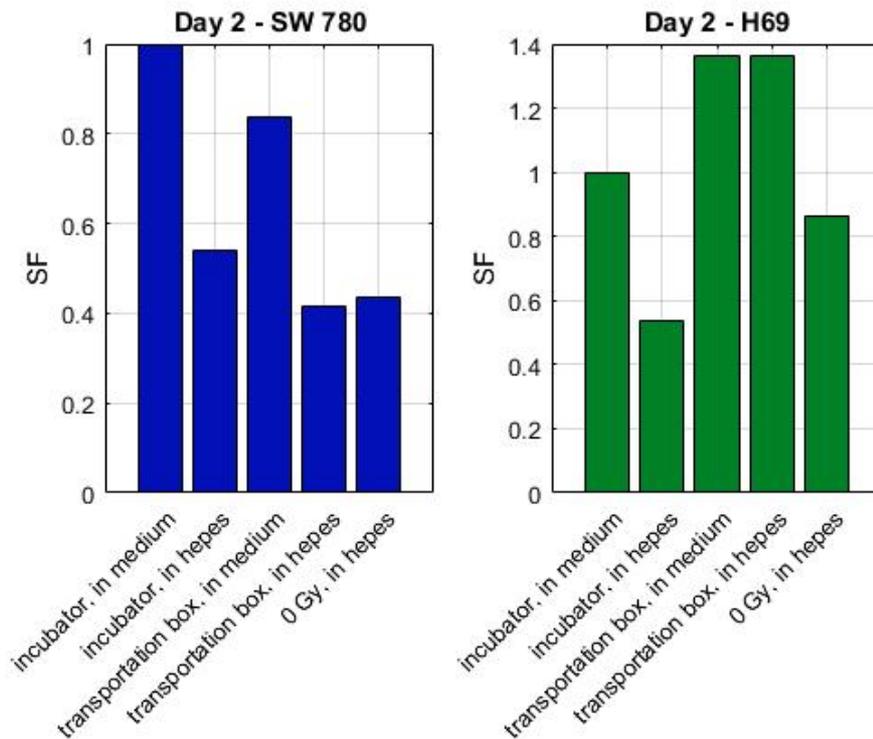
Figure 14. The measured survival fraction (SF) of SW780 and H69 cells are displayed to the left and right respectively (n=1) after two days of incubation at 37°C and 5% CO_2 after treatment. Results have been normalized to the survival obtained by cells diluted in cell culture medium and incubated at 37°C. Cells were diluted in cell culture medium ('incubator, in medium') or hepes buffer ('incubator, in hepes') and placed in an incubator at 37°C and 5% CO_2 corresponding to the time it took to transport the plates to the place of irradiation and irradiated them with 0×2, 2×2, 4×2 and 8×2 Gy in the 37°C irradiation geometry. Cells were diluted in cell culture medium ('transportation box, in medium') or hepes buffer ('transportation box, in hepes') and transported to the location of irradiation and kept in an isolated transportation box with 37°C heating blocks for the time corresponding to irradiation of 0×2, 2×2, 4×2 and 8×2 Gy in the 37°C irradiation geometry. Cells were diluted in hepes buffer and placed under the x-ray system without any applied absorbed dose ('0 Gy, in hepes') in the 37°C irradiation geometry.

In contrast to the expected outcome, cell viability was not reduced one day after treatment when cells obtained an absorbed dose greater than 2, 4, or 8 Gy compared with 0 Gy, see Figure 15. Two days after treatment, no prominent effect of radiation to the SW780 cells viability was obtained (see Figure 16), however the results indicate reduced viability for the H69 cell line in cells obtaining an absorbed dose compared with no dose, corresponding to the expected outcome.
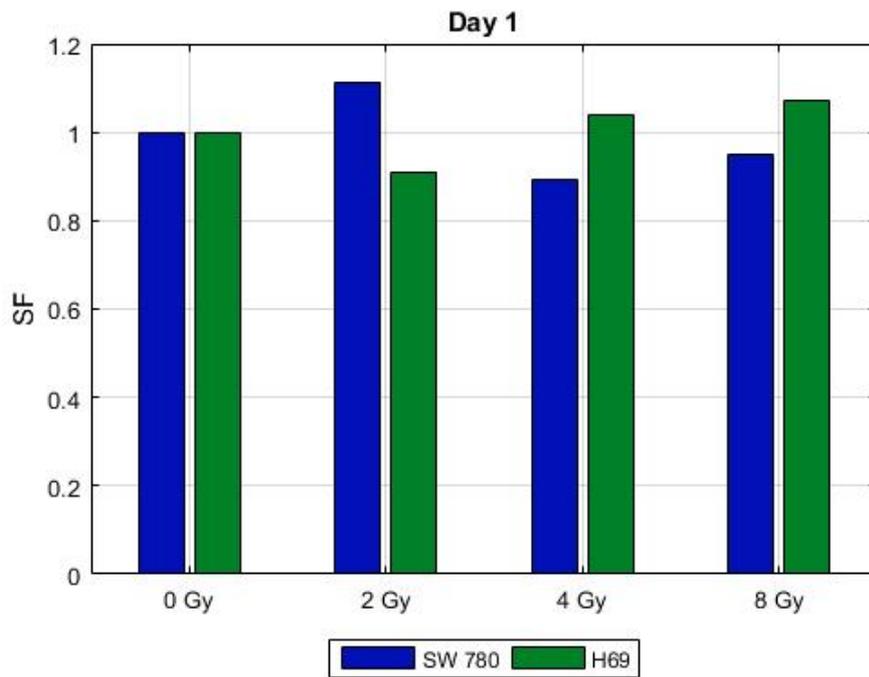
Figure 15. Survival fraction (SF), for each cell line, when the cells have obtained an absorbed dose of 0, 2, 4, and 8 Gy (n=1). Cell viability measured using a MTS viability assay one day after treatment. The obtained results for each cell line were normalized to the cell viability obtained at 0 Gy for cells treated without calcium.
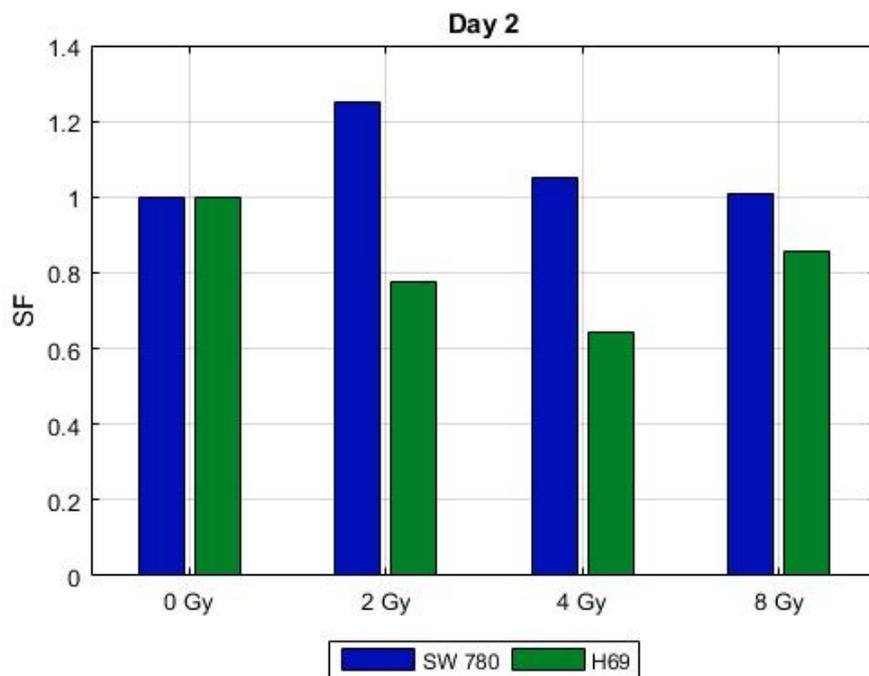

Figure 16. Survival fraction (SF), for each cell line, when the cells have obtained an absorbed dose of 0, 2, 4, and 8 Gy (n=1). Cell viability measured using a MTS viability assay two days after treatment and incubation at 37°C and 5% CO_2. The obtained results for each cell line were normalized to the cell viability obtained at 0 Gy for cells treated without calcium.

4.3.1.2   Control of the 5°C irradiation geometry

When cells from both cell lines were suspended in medium or hepes buffer and kept on ice as used for the 5°C irradiation geometry, the survival fraction was only altered very limited compared with cells suspended in cell culture medium and incubated at 37°C, see Figure 17. The viability of the cells was evaluated two days after treatment with a MTS viability assay.
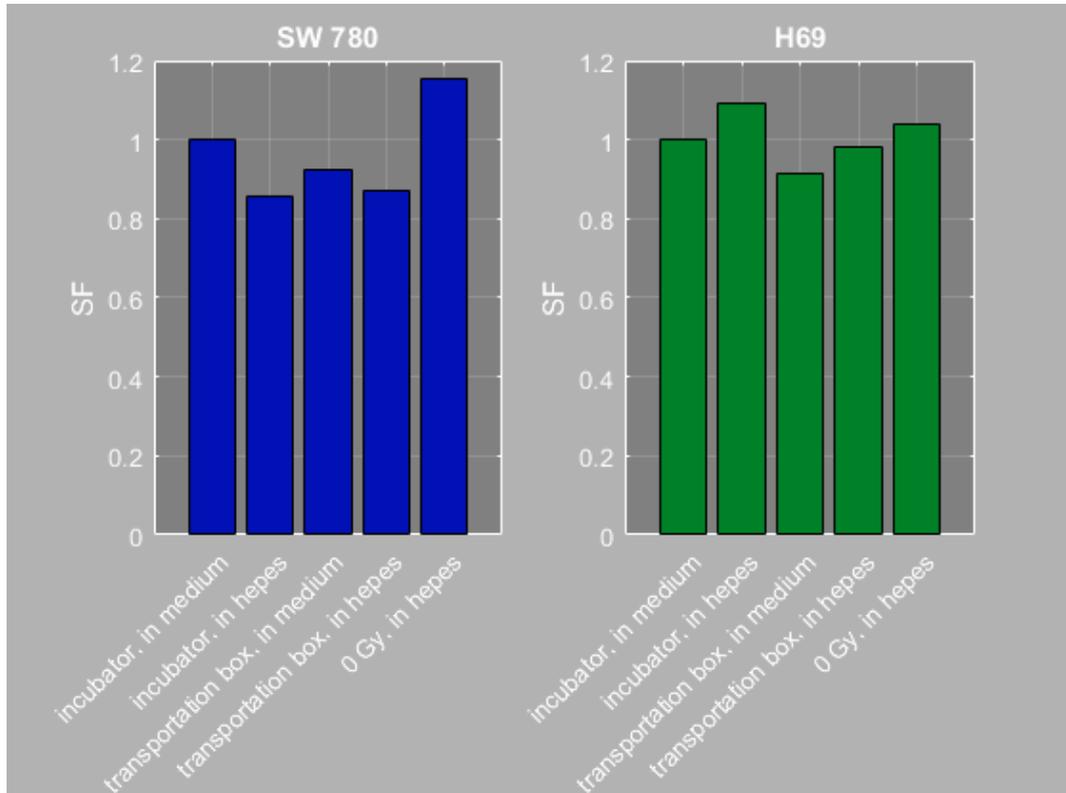

Figure 17. The measured survival fraction (SF) of SW780 and H69 cells are displayed to the left and right respectively after two days of incubation at 37°C and 5% CO_2 after treatment, n=1. Results have been normalized to the survival obtained by cells diluted in cell culture medium and incubated at 37°C. Cells were diluted in cell culture medium ('incubator, in medium') or hepes buffer ('incubator, in hepes') and placed in an incubator at 37°C and 5% CO_2 corresponding to the time it took to transport the plates to the place of irradiation and irradiated them with 0×2, 2×2, 4×2 and 8×2 Gy in the 5°C irradiation geometry. Cells were diluted in cell culture medium ('transportation box, in medium') or hepes buffer ('transportation box, in hepes') and transported to the location of irradiation and kept on ice for the time corresponding to irradiation of 0×2, 2×2, 4×2 and 8×2 Gy in the 5°C irradiation geometry. Cells were diluted in hepes buffer and placed under the x-ray system without any applied absorbed dose ('0 Gy, in hepes') in the 5°C irradiation geometry.

4.3.2   MTS Viability assay

4.3.2.1   Irradiation with Gulmay D3100

Differences in survival between cells treated with and without calcium and irradiated at the 37°C irradiation geometry is displayed for cell line SW780 and H69 in Figure 18 and Figure 19 respectively. As is displayed in Figure 18 and Figure 19 was no significant difference in survival between cells treated with and without calcium obtained for the SW780 and H69 cell line (p=0.77 and p=0.17 respectively). Each collected data point is displayed in the aforementioned figures and all data is normalized to the survival of cells exposed to 0 Gy and treated without calcium. Differences in survival for SW780 and H69 cells that obtained different absorbed doses were also investigated, however no decrease in viability could be verified for either cell line (p=1.0 and p=1.0 respectively).
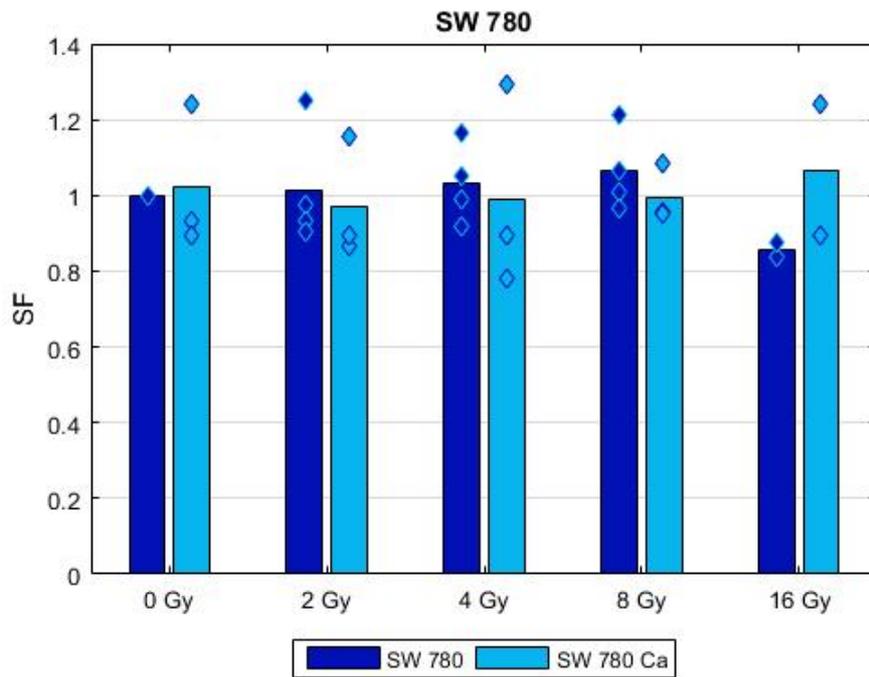
Figure 18. The mean survival (bars) for SW780 cells treated with and without calcium, which obtained an absorbed dose of 0-16 Gy at the 37°C irradiation geometry. Each collected data point (n ≥ 2) is displayed in the figure (diamond) and the collected data was normalized to the survival of the cells obtaining 0 Gy and treated without calcium.
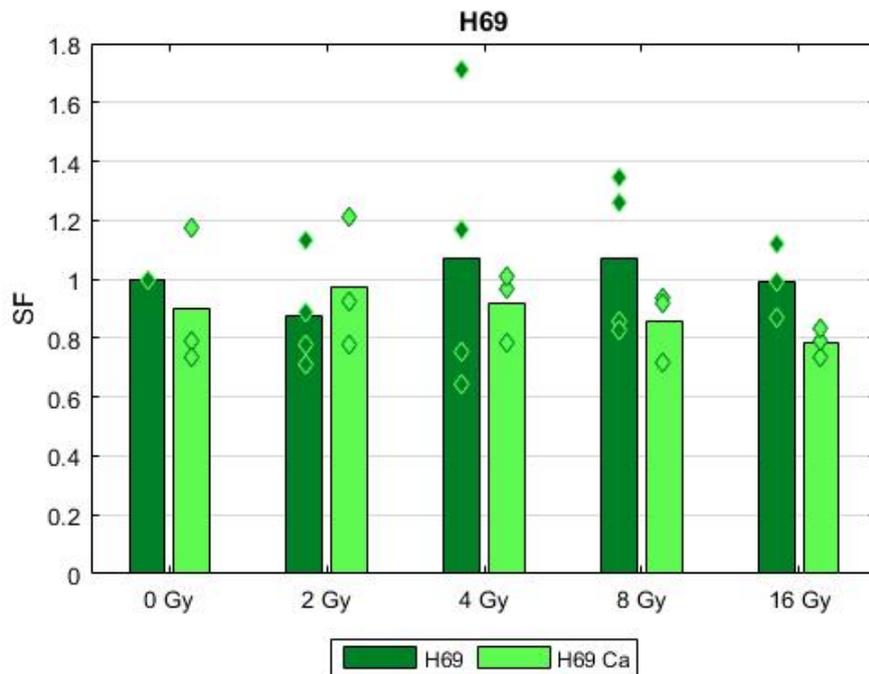

Figure 19. The mean survival (bars) for H69 cells treated with and without calcium, which obtained an absorbed dose of 0-16 Gy at the 37°C irradiation geometry. Each collected data point (n ≥ 3) is displayed in the figure (diamond) and the collected data was normalized to the survival of the cells obtaining 0 Gy and treated without calcium.

Differences in survival between cells treated with and without calcium and irradiated at the 5°C irradiation geometry are displayed for cell line SW780 and H69 in Figure 20 and Figure 21, respectively. Each collected point of data that is displayed in the aforementioned figures was normalized to the survival of the cells obtaining 0 Gy and treated without calcium. No significant difference in survival between cells treated with and without calcium was obtained for the H69 cell line (p=0.64), nevertheless was a statistic significant difference for the SW780 cell line obtained (p<0.01). The statistical analysis performed on the collected data from the SW780 cell line irradiated on ice (displayed in Figure 20) also displayed some significant differences in dose-response between the individual groups. The results obtained by the 2-way ANOVA with Bonferroni correction that displayed a difference in the mean survival that was significant is presented in Table 7. All other obtained values of p varied between 0.09 and 1.0, with a median and mean of 1.0 and 0.86 respectively. No statistical significant dose response was obtained for the H69 cell line (p=1.0).

Table 7. The obtained p-values that were less than 0.05, implying that the difference in survival between the comparing groups was significant.

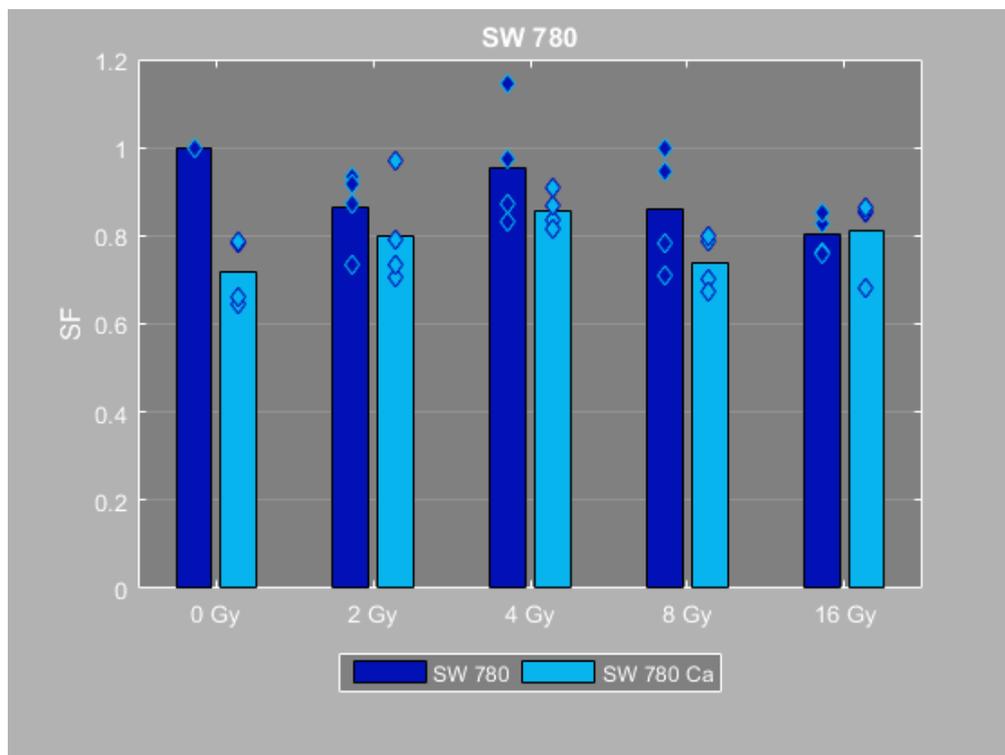|	0 Gy + 0 mM Ca	4 Gy + 0 mM Ca
0 Gy + 5 mM Ca	0.01	0.04
8 Gy + 5 mM Ca	0.01	-

Figure 20. The mean survival (bars) for SW780 cells treated with and without calcium, which obtained an absorbed dose of 0-16 Gy at the 5°C irradiation geometry. Each collected data point (n = 4) is displayed in the figure (diamond) and the collected data was normalized to the survival of the cells obtaining 0 Gy and treated without calcium.
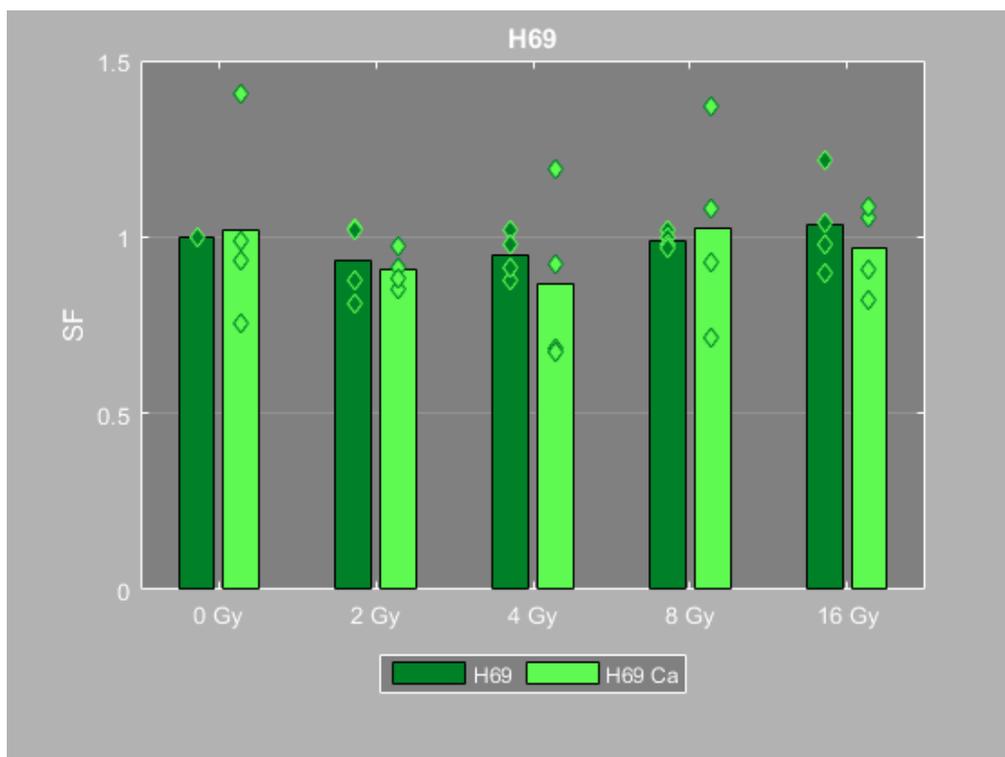
Figure 21. The mean survival (bars) for H69 cells treated with and without calcium, which obtained an absorbed dose of 0-16 Gy at the 5°C irradiation geometry. Each collected data point (n = 4) is displayed in the figure (diamond) and the collected data was normalized to the survival of the cells obtaining 0 Gy and treated without calcium.

To evaluate if the sample data for the experiments performed at the x-ray system (Gulmay D3100, Gulmay Medical) was collected from a normally distributed population the Shapiro-Wilk test was used. The obtained value of p for each cell line at the different irradiation geometry is displayed in Table 8.

Table 8. The obtained p-values from the performed Shapiro-Wilk test for the different cell lines at each irradiation geometry.

	SW780 at the 37°C irradiation geometry	H69 at the 37°C irradiation geometry	SW780 at the 5°C irradiation geometry	H69 at the 5°C irradiation geometry
p-value	0.03	0.17	0.49	0.02

4.3.2.2 Irradiation with Gulmay D3100 and Clinic IX linear accelerator

Results obtained from the irradiation of 100 Gy using the x-ray system (D3100 Gulmay, Gulmay Medical) and Varian Clinic 2300iX linear accelerator (Varian Medical Systems, Inc., Alto Palo, CA) are presented in Figure 22. The obtain survival was measured two days after treatment and normalized to the survival obtained by the cells treated without calcium and exposed to 0 Gy.
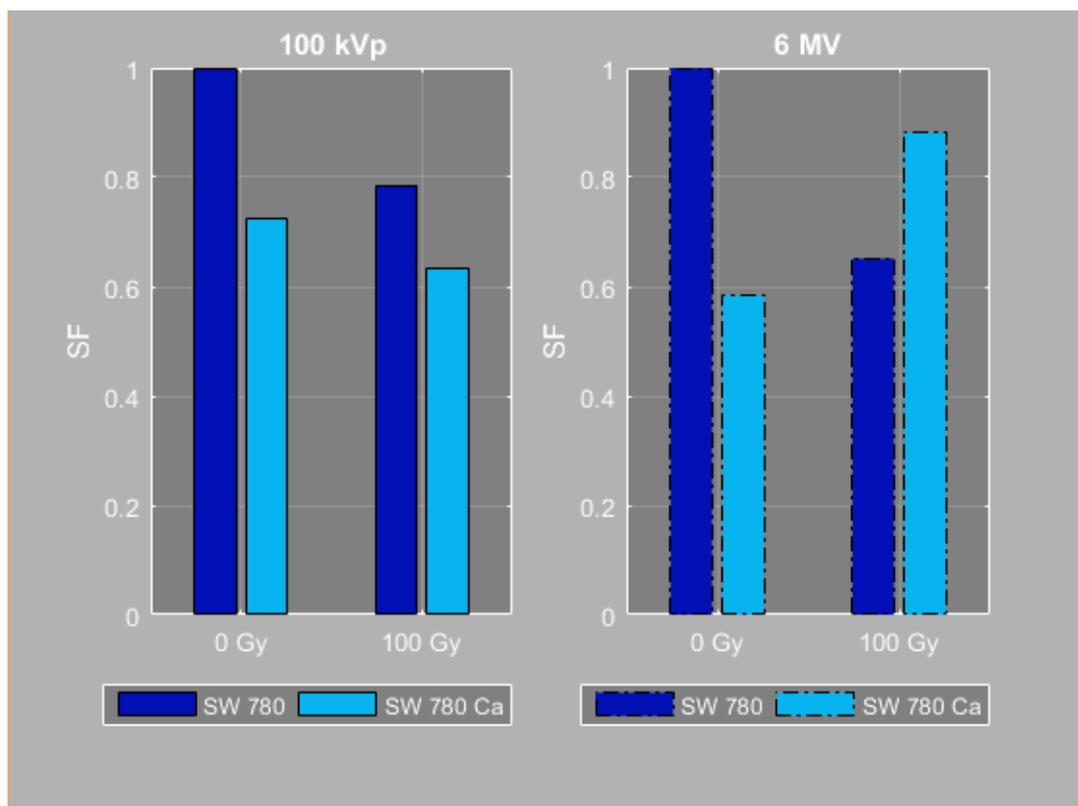
Figure 22. The measured survival of SW780 cells, treated with and without calcium, irradiated at 5°C with an absorbed dose of 100 Gy using 100 kVp x-rays generated by an x-ray Gulmay system (left) and 6 MV photons generated by a Varian 2300iX Clinic linear accelerator (right), n = 1.

4.3.3 Clonogenic assay

Presented in Figure 23 is an example of the obtained result from the performed clonogenic assay.
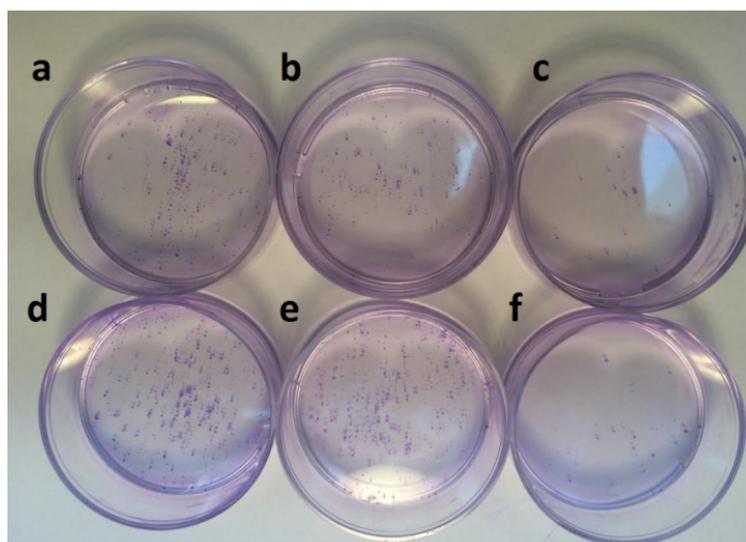

Figure 23. A clonogenic assay performed to determine the plating efficiency in a 6-well plate using SW780 cells (n = 3). (a,b) After seeding 1000 and 500 cells treated without calcium too many colonies are overlapping and the result will therefore not be reliable (c) Cells treated without calcium with 37 colonies formed after seeding 100 cells. (d,e) Too many colonies have been formed when seeding 1000 and 500 cells treated with calcium and the results are therefore not reliable. (f) Cells treated with calcium, 44 colonies are formed after seeding 100 cells.

Using equation 3 and 4 the plating efficiency (*PE*) and survival fraction (*SF)* was calculated for SW780 cells treated with and without calcium, the result is displayed in Table 9.

Table 9. The calculated plating efficiency (*PE*) and survival fraction (*SF*) for SW780 cells treated with and without calcium. *PE* is the ratio of the number of colonies to the number of seeded cells treated with and without calcium, and *SF* is the number of colonies that arise after exposure to radiation for cells treated with and without calcium.

	SW780	SW780 Ca
PE [%]	45.0	38.7
SF [%]	42.2	46.5

The expected fraction of SW780 cells surviving an absorbed dose of 4 Gy was calculated, using a α/β-value of 6.2 for bladder cancer cells proposed by literature [34] and equation 5, to approximately 10%.

4.4 Discussion

4.4.1 Controls

4.4.1.1 Controls of the 37°C irradiation geometry

From Figure 13, it can be concluded that the most optimal environment for the SW780 cells are to be suspended in cell culture medium. It is also observed that the difference in growth between the cells diluted in cell culture medium and exposed to different conditions, kept in the incubator at 37°C and 5% CO_2 or kept in a transportation box at a temperature of 37°C, is not prominent. Survival of the SW780 cells is affected when diluted in hepes buffer, approximately 50% of the cells die because of this treatment regardless if they are kept in the incubator, transportation box, or irradiated with 0 Gy (see Figure 13). Nevertheless does the obtained result imply that the other external conditions, such as temperature and carbon dioxide concentration, do not extensively affect the survival of the SW780 cells suspended in hepes buffer.

As displayed in Figure 14 do the results for the SW780 cell line incubated for two days after treatment correspond with the results obtained one day after treatment. Two differences are observed; first the survival rate of SW780 cells diluted in cell culture medium and kept in the incubator (i.e. the control) is somewhat greater than cells diluted in cell culture medium and kept at the transportation box. Secondly the survival rate of cells diluted in hepes buffer and kept in the transportation box or irradiated with 0 Gy is reduced to around 40% of the control.

The growth of H69 cells is optimal when the cells are diluted in cell culture medium and kept in the incubator at 37°C and 5% CO_2, see Figure 13. Even though the survival of cells suspended in cell culture medium is reduced when they are kept in the transportation box this survival rate is equivalent to that of H69 cells kept in the transportation box at 37°C and suspended in hepes buffer. As can be seen in Figure 13 is the survival of H69 cells that were exposed to an absorbed dose of 0 Gy and suspended in hepes buffer reduced. The possible explanation for this is that the change in temperature, occurring when adjacent wells on the 96-well plate were irradiated, affected the growth of the cells, reducing the survival of the H69 cells by 50%. It is also possible that the dose contribution, due to scatter from the irradiated adjacent wells, affects the cells. This is however considered improbable as the dose contribution due to scatter was investigated and concluded insignificant small, see section *3.4.2 TLD*. As is displayed in Figure 13 is the survival of cells suspended in hepes buffer and incubated at 37°C and 5% CO_2 in the same range of the survival of the cells irradiated with 0 Gy. A probable

explanation for this result is that the 5% CO_2 in the incubator might decrease the pH of the hepes buffer and create a less optimal environment for the cells. Even though the cells transported to the location of irradiation were kept at a temperature close to 37°C is the level of CO_2 in air lower than 5%.

Survival of the H69 cell line incubated for two days after treatment at 37°C and 5% CO_2 does also to some extent correspond with the obtained result one day after treatment; see Figure 14 and Figure 13 respectively. One obtained difference is that the survival rate of cells kept in the transportation box was greater than cells diluted in cell culture medium and kept at an incubator. This was unexpected since the optimal condition for cells are in cell medium kept in an incubator at 37°C and 5% CO_2. A probable reason for the increased survival rate in the cells kept in the transportation box could be that the cells increase their metabolism when they sence a change in the conditions to be able to cope with these changes, and this increased metabolism will be shown as an increased survival rate when using MTS assay. However more experiments are needed to verify the obtained results as this experiment only was performed once.

The dose response one day after treatment with and without calcium and increasing absorbed doses of the SW780 cells and the H69 cells was not as expected, as no notable decrease in survival was noted as the obtained absorbed dose to the cells was increased, see Figure 15. Cell death initiated by exposure to ionizing radiation occurs most frequently by mitotic death, which is classified as a post-mitotic cell death and occurs a few cell cycles after exposure. The doubling times for the cells used in this study were 1.2 days and 1.85 days for SW780 and H69 cell line, respectively. Thus, one or two days of incubation at 37°C and 5% CO_2 are therefore likely not enough to study the response of radiation. Two days of incubation at 37°C and 5% CO_2 after treatment was also tested and as seen in Figure 16 and a possible dose response for cell line H69 was obtained, however a dose response for the SW780 cell line was not obtained. This could indicate that small cell lung cancer cells (H69 cells) are more radiosensitive than bladder cancer cells (SW780 cells), however in order to confirm this hypothesis the experiment must be repeated. It is also possible that H69 cells to a larger extent undergo cell death after irradiation through e.g. necrosis or apoptosis, which are cell death mechanisms that manifest faster than mitotic cell death. Even though no noteworthy dose response was obtained, it was expected that the obtained absorbed dose would permeabilize the plasma membrane why an effect of the calcium injections still should be noticeable as the effect of an increased intracellular concentration of calcium previously has been manifested one and two days after treatment when using calcium electroporation [10], [11], [14], [35]. Due to the fact that radiation most frequently initiates post-mitotic cell death, it was decided that the viability of the cells would be evaluated two days after treatment in the remaining experiments. It can be argued that the number of days the cells were incubated after treatment should have been increased; however this introduced a number of practical difficulties. First must the cell culture medium be changed several times and since the H69 cells are growing as spherical floating aggregates they risked being removed along with the medium even though the H69 cells can be spun down by centrifuging the 96-well plates. Another limitation was the limited time frame of the study, by reducing the number of days of incubation results could be obtained and evaluated earlier, thus allowing a greater number of experiments to be performed. This was also the reason why clonogenic assay was not the standard method used to measure the viability of cells in this study.

4.4.1.2 Control of the 5°C irradiation geometry

Due to the relatively high cell death of cells suspended in hepes buffer using the 37°C irradiation geometry the effect of using a 5°C irradiation geometry was tested, since a high cell survival of untreated control cells is preferred.

From the obtained result in Figure 17, it can be concluded that the significance of the medium/buffer SW780 cells were suspended in and the different conditions they were exposed to, reduce when the experiment was performed in the 5°C irradiation geometry. A probable explanation for this is that the metabolic activity of the cells reduces when they are kept on ice and therefore are the external conditions of less importance. The obtained result for cell line SW780 also indicates that the time the cells irradiated with 0 Gy spend in room temperature in this study does not affect the cells capability to grow. From Figure 17, it can be concluded that there are no prominent differences in survival of H69 cells exposed to different conditions. It is thus concluded that the H69 cell line is resilient and can withstand the external strains the 5°C irradiation geometry entails. Putting the cells on ice slows down the metabolic rate and the result inclines that this is enough to reduce the differences in the survival for cells exposed to different external environments.

Based on the results found in Figure 13, Figure 14 and Figure 17, it can be concluded that for either cell line in the 37°C irradiation geometry the cell culture medium is the most ideal medium for the cells to be diluted in. It is also determined that the obtained difference in survival, depending on the medium the cells are suspended in, is not prominent for either cell line for the 5°C irradiation geometry. Unfortunately the cells could not be suspended in cell culture medium when the effect of calcium injections was investigated due to the fact that the cell culture medium contains calcium. Experiments without calcium could therefore not be performed if using medium, and since several calcium electroporation experiments have previously used cells diluted in hepes buffer [10], [11], [14], this buffer was chosen to be the standard for this study.

From Figure 14 and Figure 17, it can be concluded that when the experiment was performed at the 5°C irradiation geometry the external conditions did not affect the cell survival to the same extent as when the experiments was performed at the 37°C irradiation geometry. The obtained results from the 5°C irradiation geometry should therefore be more reliable since the untreated control cells did not die. Nevertheless would it be ideal to perform the experiment at 37°C as this corresponds to the body temperature and thereby the ideal temperature of the cells. There might also be other features that are influenced by the lowered temperature, e.g. the rigidity and thereby the permeability of the membranes, and this might act as a confounding factor.

4.4.2 MTS viability assay

4.4.2.1 Irradiation with Gulmay D3100

No statistical significant difference in survival between SW780 cells treated with and without calcium in the 37°C irradiation geometry was obtained (p=0.77), see Figure 18. As is also displayed in Figure 18 was no significant difference in survival between cells that were irradiated with different doses observed (p=1.0).

A minor difference in survival between H69 cells treated with and without calcium and irradiated at the 37°C irradiation geometry appears to be observed in Figure 19, however the difference is not significant (p=0.17) and moreover this minor difference is also observed for cells that obtained an

absorbed dose of 0 Gy. Exposing the H69 cells to radiation does not affect the survival of the cells (p=1.0) and the expected decrease in survival is not observed when the absorbed dose is increased, see Figure 19.

From Figure 20 and the statistical analysis that was performed it can be concluded that a statistically significant difference (p=0.0005) in survival between SW780 cells treated with and without calcium was obtained using the 5°C irradiation geometry. A relative decrease in survival rate can be observed for cells treated with calcium and exposed to 0-8 Gy compared with cells treated without calcium, see Figure 20. As a decrease in survival is observed for cells treated with calcium compared with cells treated without calcium obtaining 0 Gy and not 16 Gy, it is assumed that the result is not due to the concurrent effect of radiation and calcium but only displays the effect of calcium alone. Calcium is involved in many cellular processes, e.g. proliferation and cell death. An observed increased survival rate for cells irradiated with 16 Gy may thus be explained by calcium acting as a growth signal. This explanation does however contradicts the result obtained by Hansen et al. [11] that indicates that the survival rate of the SW780 or H69 cell line is not affected by calcium treatment alone. The statistically significantly reduced viability is thus considered to be a result of the low number of performed experiments in this study. This conclusion is further verified by the result obtained in Table 7 as the differences in survival between groups that obtained 0 Gy and different concentrations of calcium were statistical significant. For the 5°C irradiation geometry and the SW780 cell line, a dose response were observed between some of the groups, see Table 7. The survival of cells treated with calcium and irradiated with 8 Gy was significantly lower than the survival rate of cells irradiated with 0 Gy and treated without calcium. One can argue that this indicates an effect of concurrent radiation and calcium, however no significant difference in survival between untreated cells obtaining 0 Gy and cells treated with calcium receiving higher or lower doses was establish. It is therefore considered unlikely that the result displays an effect of concurrent radiation and calcium. An explanation for the result may be that the few number of collected data points do not reflect the population. It is also possible that the effect is a result of calcium alone. To verify this hypothesis collection of more data is necessary.

Assessing the viability of H69 cells irradiated at the 5°C irradiation geometry showed that no difference in survival rate between cells treated with and without calcium was obtained (p=0.64), see Figure 21. No dose response, regardless of the calcium concentration, could be observed (p=1.0) in the collected data.

There are several possible explanations for why an effect of concurrent radiation and calcium was not observed. Firstly, it is possible that the permeabilization by peroxidation of the cellular membrane is not substantial for a high enough calcium concentration to enter the cell and initiate cell death. To verify this hypothesis an experiment where cells are irradiated in a buffer containing a dye, e.g. propidium iodide, could have been performed. Examining the colour of the cells after an irradiation using a microscope it could have been determined whether the permeabilization of the membrane was enough to increase the intracellular concentration of calcium to a dangerously high level and initiate cell death. Secondly, it is possible that the cell membrane becomes permeabilized to such a degree that calcium enters the cell and that the cell survives this external strain. However, this explanation is not considered likely as results from calcium electroporation experiments performed with the same calcium concentration used in this study display a reduced cell viability [10], [11], [14], [35]. *A calcium concentration of 5 mM is therefore considered to be high enough to initiate cell death and influence the cell viability.* Another possible explanation for the obtained result is that calcium enters the cells through the permeabilized membrane but initiate a slow cell death that still have not manifested two

days after treatment. This could be investigated using clonogenic assay. To summarize, the permeabilization of the cell membrane could not be verified and it cannot be excluded that the concurrent effect of radiation and calcium initiate damages that do not initiate cell death within two days. The recommendation of the author is therefore to perform the experiment again using a buffer containing dye and clonogenic assay.

4.4.2.2   Dose response

As is observed in Figure 18-Figure 21, no dose response was detected with increasing irradiation when using a MTS viability assay to assess the viability of the treated cells. This is explained by the fact that ionizing radiation to a large extent initiates cell death by mitotic catastrophe, which is a post-mitotic cell death and takes place several cell cycles after the irradiation. Therefore, cells that are predetermined to die will still be assessed as viable two days after the irradiation using the MTS assay as the cells still are metabolic active even though they have lost their ability to divide. This was not considered a problem as results from calcium electroporation experiments performed with the same calcium concentration used in this study, displayed drastically reduced survival already one day after treatment [10], [11], [14], [35]. However, this expected reduced cell survival was not obtained and it is therefore necessary to reconsider the method used to measure the viability. It is concluded that the MTS viability assay is likely not a preferable method to assess viability of the cells in this study since no effect of the absorbed dose was obtained. The recommendation of the author is thus that this study is to be performed again using clonogenic assay to measure the cells ability to divide, which should produce more reliable results. To summarize, the result of this study is that by using MTS assay no evidences of an increased cellular influx of calcium to levels initiating cell death through the permeabilized cell membrane were found. However, as no dose-response could be detected using the MTS assay the existence of a concurrent effect of radiation and calcium could not be excluded without further investigations; preferably using clonogenic assay, where a dose response for the dosage and cell line used can be expected [36].

Variations in the collected sets of data were obtained (see Figure 18-Figure 21) and each collected point of data was displayed instead of the standard deviation of the sample. As only four points of data were collected for each absorbed dose in the different irradiation geometries the display of each collected point of data was regarded as a better way to present the variations within the obtained data.

4.4.2.3   Statistical analysis

As is displayed in Table 8, the null hypothesis could be rejected in two cases using the Shapiro-Wilk test, used to examine if the samples were collected from a population that was normally distributed. Despite this obtained result, it was decided that the statistical analyses were to be performed using a 2-way Analysis of Variance (ANOVA) with a Bonferroni correction. ANOVA is an extension of the parametric t-test and one of the conditions or assumptions that underlie a t-test is that the collected set of data follows an approximately normally distributed variable. The need to fulfil this condition can be neglected if the number of observations is great, however the collected number of measurement points were few and the application of a parametric test can therefore not be justified using this exception. Nonetheless having a few number of measurement points makes it difficult to prove that the samples are collected from a population that is normally distributed. Using a non-parametric test has therefore been considered, since it would result in a better statistical power. It was however assumed that the population of the sample was normally distributed and that if more data was collected this would have been verified. It was therefore decided that a 2-way ANOVA with Bonferroni correction could be performed.

4.4.3   Irradiation with Gulmay D3100 and Clinic IX linear accelerator

In order to verify the dose delivery of the x-ray system and to further investigate the adequacy of the MTS viability assay one experiment was performed were the cells plated out in the 96-well plate received an absorbed dose of 100 Gy using the x-ray system (Gulmay D3100, Gulmay Medical) and a Varian 2300iX Clinic linear accelerator (Varian Medical Systems, Inc., Alto Palo, CA). Due to the extensive irradiation time, this experiment was only performed for the SW780 cell line. As is displayed in Figure 22, a difference in survival between the cells that obtained 0 Gy or 100 Gy was observed regardless of the source of radiation, however the difference was not as great as expected as 100 Gy should eradicate all living cells. This is a further verification that the method used to measure the viability of the cells is inappropriate. It seems, from Figure 22, that the dose response of the cells treated with calcium is somewhat different depending on the source of radiation. If this result is obtained as a response to the different dose rates or if it was obtained by chance needs to be determined by further investigations as this experiment only was performed once. The results presented in Figure 22 also confirm the dose delivery of the x-ray system since the cell survival of the x-ray system in general corresponds to that of the Varian 2300iX Clinic linear accelerator.

4.4.4   Clonogenic assay

As is displayed in Table 9, the survival rate for SW780 cells treated with and without calcium was affected by the obtained absorbed dose as the survival was decreased to approximately 45% . This obtained survival rate was greater than the expected survival rate of 10 % for bladder cancer cells treated with 4 Gy. It is possible that the proposed α/β-value from literature that was used to estimate the survival was not based on the same cell line and that the α/β-value cannot be applied for the SW780 cell line. Even though the 6-well plate during the time of irradiation was surrounded by ice there was still air surrounding the cells as the area around the wells in a 6-well plate was not filled with ice due to an increased risk of contaminating the samples. This will affect the delivered absorbed dose to the cells and thereby the survival rate as the scatter contribution to the absorbed dose from air is less than water. The mass energy absorption coefficient for plastic relative to water depends on the energy, the energy fluence spectra change with field size and depth and is therefore not constant. Using plastic (PMMA) will introduce uncertainties in the dose delivery as the absorbed dose will be dependent on the spectrum of the beam and the mass energy absorption coefficient from the plastic material relative to water. Another explanation for the unexpected great survival rate is that the observer may have made an error counting the formed colonies in the wells. It is also possible that some colonies have been removed together with the hepes buffer, cell culture medium, or PBS during the experiment. However, a dose response was indubitable observed and it is therefore concluded that if the effect of concurrent radiation and calcium should be investigated any further it is recommended that the viability is determined by a clonogenic assay. If the experiment was to be performed again, factors such as the number of days in incubation after treatment and the concentration of cells in the wells should be investigated in order to optimize the procedure.

From Table 9, it seems that no difference in survival between cells treated with and without calcium was obtained, however it is the opinion of the author that more experiments are required to determine whether this result was significant or obtained by chance. When repeating the experiment, it is also recommended that the standard procedure evaluating combinations of radiation with other treatments is used, i.e. a radiation dose-survival curve is obtained and a dose enhancement ratio is determined.

4.5   Conclusion

When using a MTS viability assay to study the cell viability two days after treatment, no differences in survival rate of cells treated with and without calcium in combination with radiotherapy were obtained. It is concluded that the acute damage of the plasma membrane is not enough to permeabilize the cell membrane to such a degree that the cell viability is reduced. However effect of concurrent radiation and calcium could not thoroughly be investigated due to the chosen method of measuring the cells viability. Further investigations, preferably using clonogenic assay where the ability to divide can be observed, and experiments using a coloured dye instead of calcium are therefore necessary before the hypothesis can be rejected. Nonetheless it can be concluded that when using a colorimetric assay no evidence of a concurrent effect of radiation and calcium were found and that the effect does not seems to be influenced by the absorbed dose.

5. Future aspects

This work constitutes an initial foundation for investigating the effect of concurrent radiation and calcium, however to further investigate the impact of calcium in combination with radiotherapy the results need to be evaluated using clonogenic assay. To investigate the impact of different concentrations of calcium, obtained absorbed doses, fractionation patterns and dose rates would also be of interest in this context.

6. Acknowledgement

Finally thanks to my boyfriend, family and friends for your encouragement and words of wisdom. SH you are truly my source of inspiration and my biggest supporter, without you this project would not have been possible.

7. Bibliography
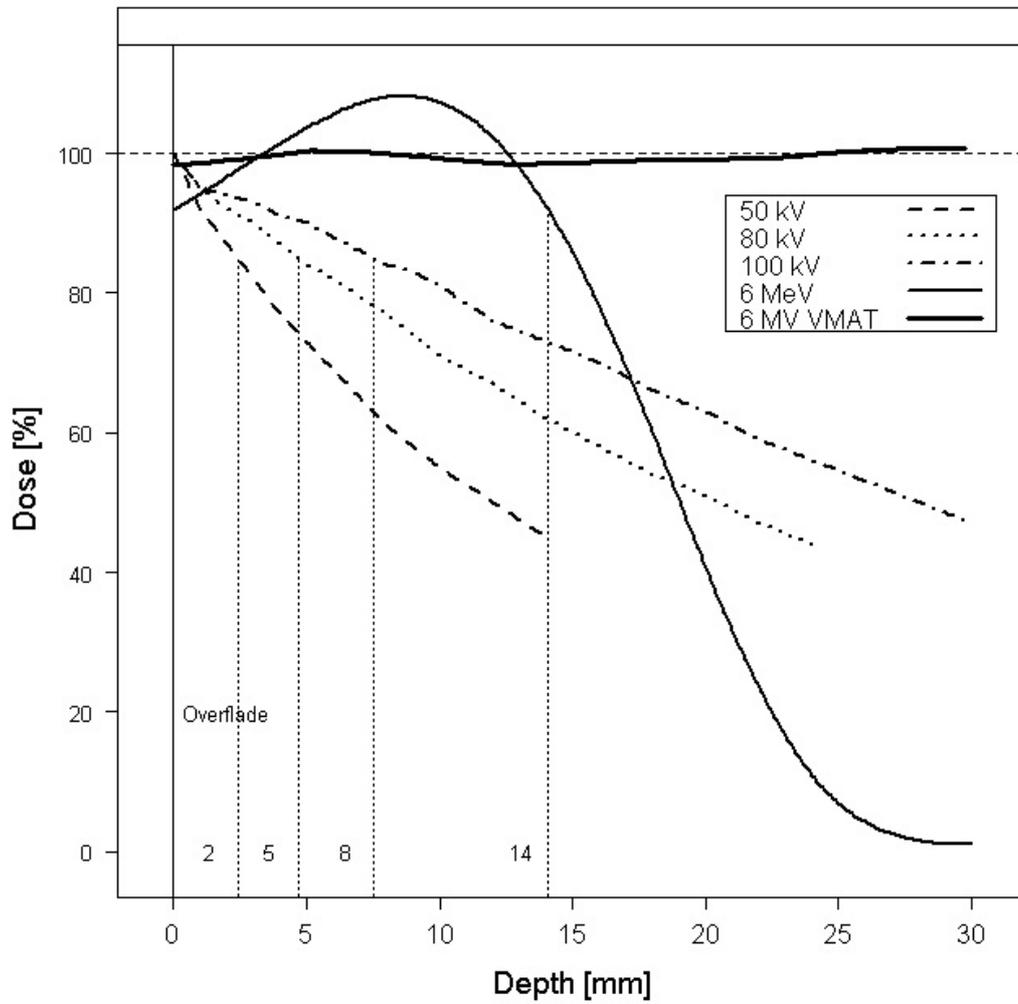
[1]   D. Shier, J. Butler, and R. Lewis, *Hole's essentials of Human Anatomy & Physiology*, vol. 10. 2009.

[2]   L. Hallstadius and S. Hertzman, *Joniserande strålnings växelverkan med materia*. Radiofysiska institutionen, Lunds Universitet, 1984.

[3]   K. D. Held, "Radiobiology for the Radiologist, 6th ed., by Eric J. Hall and Amato J. Giaccia," *Radiation Research*, vol. 166, no. 5. pp. 816–817, 2006.

[4]   G. Barrera, "Oxidative Stress and Lipid Peroxidation Products in Cancer Progression and Therapy," *ISRN Oncol.*, vol. 2012, pp. 1–21, 2012.

[5]   B. D. Lawenda, K. M. Kelly, E. J. Ladas, S. M. Sagar, A. Vickers, and J. B. Blumberg, "Should Supplemental Antioxidant Administration Be Avoided During Chemotherapy and Radiation Therapy?," *JNCI J. Natl. Cancer Inst.*, vol. 100, no. 11, pp. 773–783, Jun. 2008.

[6]   A. van der Kogel, *Basic Clinical Radiobiology*, Fourth Edi. CRC Press, 2009.

[7]   E. Carafoli, L. Santella, D. Branca, and M. Brini, "Generation, control, and processing of cellular calcium signals," *Crit Rev Biochem Mol Biol*, vol. 36, no. 2, pp. 107–260, 2001.

[8]   C. H. Mitchell, D. a Carré, a M. McGlinn, R. a Stone, and M. M. Civan, "A release mechanism for stored ATP in ocular ciliary epithelial cells.," *Proc. Natl. Acad. Sci. U. S. A.*, vol. 95, no. 12, pp. 7174–7178, 1998.

[9]   W. Wu, P. Liu, and J. Li, "Necroptosis: An emerging form of programmed cell death," *Crit. Rev. Oncol. Hematol.*, vol. 82, no. 3, pp. 249–258, 2012.

[10]   S. K. Frandsen, H. Gissel, P. Hojman, T. Tramm, J. Eriksen, and J. Gehl, "Direct Therapeutic Applications of Calcium Electroporation to Effectively Induce Tumor Necrosis," *Cancer Res.*, vol. 72, no. 6, pp. 1336–1341, Mar. 2012.

[11]   E. L. Hansen, E. B. Sozer, S. Romeo, S. K. Frandsen, P. T. Vernier, and J. Gehl, "Dose-Dependent ATP Depletion and Cancer Cell Death following Calcium Electroporation, Relative Effect of Calcium Concentration and Electric Field Strength," *PLoS One*, vol. 10, no. 4, p. e0122973, Apr. 2015.

[12]   G. Cao, M. Zhang, J. Miao, W. Li, J. Wang, D. Lu, and J. Xia, "Effects of X-ray and carbon ion beam irradiation on membrane permeability and integrity in Saccharomyces cerevisiae cells," *J. Radiat. Res.*, vol. 56, no. 2, pp. 294–304, Mar. 2015.

[13]   S. Jouan-Lanhouet, M. I. Arshad, C. Piquet-Pellorce, C. Martin-Chouly, G. Le Moigne-Muller, F. Van Herreweghe, N. Takahashi, O. Sergent, D. Lagadic-Gossmann, P. Vandenabeele, M. Samson, and M.-T. Dimanche-Boitrel, "TRAIL induces necroptosis involving RIPK1/RIPK3-dependent PARP-1 activation," *Cell Death Differ.*, vol. 19, no. 12, pp. 2003–2014, Dec. 2012.

[14]   S. K. Frandsen, H. Gissel, P. Hojman, J. Eriksen, and J. Gehl, "Calcium electroporation in three cell lines: a comparison of bleomycin and calcium, calcium compounds, and pulsing conditions," *Biochim. Biophys. Acta (BBA)-General Subj.*, vol. 1840, no. 3, pp. 1204–1208, 2014.

[15]   M. Brini and E. Carafoli, "Calcium signalling: a historical account, recent developments and future

perspectives," *Cell. Mol. Life Sci.*, vol. 57, no. 3, pp. 354–370, 2000.

[16]   G. Stark, "The effect of ionizing radiation on lipid membranes.," *Biochim. Biophys. Acta*, vol. 1071, no. 2, pp. 103–22, Jul. 1991.

[17]   W. A. Cramp, M. B. Yatvin, and M. Harms-Ringdahl, "Recent Developments in the Radiobiology of Cellular Membranes," *Acta Oncol. (Madr).*, vol. 33, no. 8, pp. 945–952, Jan. 1994.

[18]   J. Hannig, D. Zhang, D. J. Canaday, M. a Beckett, R. D. Astumian, R. R. Weichselbaum, and R. C. Lee, "Surfactant sealing of membranes permeabilized by ionizing radiation.," *Radiat. Res.*, vol. 154, no. 2, pp. 171–7, Aug. 2000.

[19]   G. J. Köteles, "Radiation Effects on Cell Membranes," *Radiat. Environ. Biophys.*, vol. 21, no. September 1981, pp. 1–18, 1982.

[20]   L. Ouyang, Z. Shi, S. Zhao, F. T. Wang, T. T. Zhou, B. Liu, and J. K. Bao, "Programmed cell death pathways in cancer: A review of apoptosis, autophagy and programmed necrosis," *Cell Prolif.*, vol. 45, no. 6, pp. 487–498, 2012.

[21]   M. N. Cornforth and J. S. Bedford, "A quantitative comparison of potentially lethal damage repair and the rejoining of interphase chromosome breaks in low passage normal human fibroblasts.," *Radiat. Res.*, vol. 111, no. 3, pp. 385–405, 1987.

[22]   E. I. Azzam, J.-P. Jay-Gerin, and D. Pain, "Ionizing radiation-induced metabolic oxidative stress and prolonged cell injury," *Cancer Lett.*, vol. 327, no. 1–2, pp. 48–60, Dec. 2012.

[23]   A. Petkau, "Role of superoxide dismutase in modification of radiation injury.," *Br. J. Cancer. Suppl.*, vol. 8, pp. 87–95, 1987.

[24]   I. Pearson Education, "Cell membrane," *http://cmapspublic2.ihmc.us/servlet/SBReadResourceServlet?rid=1165370235261_270731183_6417*, 2003. .

[25]   J. Gehl, "Electroporation: theory and methods, perspectives for drug delivery, gene theraphy and research," *Acta Physiol. Scand.*, vol. 177, no. 4, pp. 437–447, 2003.

[26]   E. Carafoli, "The calcium pump of the plasma membrane," *J. Mol. Cell. Cardiol.*, vol. 24, no. I, p. 33, May 1992.

[27]   T. L. Riss, R. A. Moravec, A. L. Niles, H. A. Benink, T. J. Worzella, and L. Minor, "Cell viability assays," *Assay Guid. Man.*, 2013.

[28]   N. a P. Franken, H. M. Rodermond, J. Stap, J. Haveman, and C. van Bree, "Clonogenic assay of cells in vitro.," *Nat. Protoc.*, vol. 1, no. 5, pp. 2315–9, 2006.

[29]   G. F. Knoll, "Thermoluminescent dosimeters and image plates," in *Radiation detection and measurement*, 4th ed., John Wiley & Sons, Inc, 2010, pp. 751–758.

[30]   V. C. Borca, M. Pasquino, G. Russo, P. Grosso, D. Cante, P. Sciacero, G. Girelli, M. Rosa, L. Porta, and S. Tofani, "Dosimetric characterization and use of GAFCHROMIC EBT3 film for IMRT dose verification," *J. Appl. Clin. Med. Phys.*, vol. 14, no. 2, pp. 158–171, 2013.

[31]   L. J. van Battum, D. Hoffmans, H. Piersma, and S. Heukelom, "Accurate dosimetry with GafChromic EBT film of a 6 MV photon beam in water: What level is achievable?," *Med. Phys.*, vol. 35, no. 704, pp. 704–716, 2008.

[32] E. Aksamitiene, "Cell Signaling Networks," *http://www.cellsignet.com/media/templ.html*, 2009. .

[33] T. D. Sterling, H. Perry, and L. Katz, "Automation of Radiation Treatment Planning—IV. Derivation of a Mathematical Expression for the per cent Depth Dose Surface of Cobalt 60 Beams and Visualisation of Multiple Field Dose Distributions," *Br. J. Radiol.*, vol. 37, no. 439, pp. 544–550, 1964.

[34] A. Nahum and D. Chapman, *Radiotherapy Treatment Planning - linear-quadratic radiobiology*. CRC Press, 2015.

[35] S. K. Frandsen, L. Gibot, M. Madi, J. Gehl, and M.-P. Rols, "Calcium Electroporation: Evidence for Differential Effects in Normal and Malignant Cell Lines, Evaluated in a 3D Spheroid Model," *PLoS One*, vol. 10, no. 12, p. e0144028, Dec. 2015.

[36] F. Mendes, T. Sales, C. Domingues, S. Schugk, A. M. Abrantes, A. C. Gonçalves, R. Teixo, R. Silva, J. Casalta-Lopes, C. Rocha, M. Laranjo, P. C. Simões, A. B. S. Ribeiro, M. F. Botelho, and M. S. Rosa, "Effects of X-radiation on lung cancer cells: the interplay between oxidative stress and P53 levels.," *Med. Oncol.*, vol. 32, no. 12, p. 266, Dec. 2015.

Appendix 1

The depth dose curve of the x-ray system (Gulmay D3100, Gulmay Medical) that was used to generate the 100 kVp x-rays is presented in A1.

A1. The depth dose curve for the x-ray system (Gulmay D3100, Gulmay Medical) used during the study. Courtesy of Jens Edmund, Herlev Hospital.